Journal of Water Process Engineering 57 (2024) 104645

Contents lists available at ScienceDirect

Journal of Water Process Engineering

journal homepage: www.elsevier.com/locate/jwpe

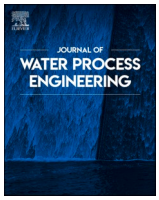

# CQDs embed g-$C_3N_4$ photocatalyst in dye removal and hydrogen evolution: An insight review

Solayman H. M. [a], Azrina Abd Aziz [a,b,*], Noor Yahida Yahya [a], Kah Hon Leong [c], Lan Ching Sim [d], Md. Kamal Hossain [e], Md. Badiuzzaman Khan [f], Kyung-Duk Zoh [g]

[a] Faculty of Civil Engineering Technology, Universiti Malaysia Pahang Al-Sultan Abdullah, 26300 Gambang, Pahang, Malaysia
[b] Advanced Intelligent Materials Centre, Universiti Malaysia Pahang Al-Sultan Abdullah, 26300 Gambang, Pahang, Malaysia
[c] Department of Environmental Engineering, Faculty of Engineering and Green Technology, Universiti Tunku Abdul Rahman, 31900 Kampar, Perak, Malaysia
[d] Department of Chemical Engineering, Lee Kong Chian Faculty of Engineering and Science, Universiti Tunku Abdul Rahman, 43200 Kajang, Selangor, Malaysia
[e] Bangladesh Council of Scientific and Industrial Research, BCSIR Laboratories, Dhaka 1205, Bangladesh
[f] Department of Environmental Science, Bangladesh Agricultural University, Mymensingh 2202, Bangladesh
[g] Department of Environmental Health Sciences, School of Public Health, Seoul National University, Seoul 151-742, Republic of Korea

ARTICLE INFO

*Keywords:*
CQDs
g-$C_3N_4$
Photocatalysis
Hydrogen evolution
Dye wastewater treatment

ABSTRACT

Recent research has highlighted heterogeneous photocatalysts as a feasible contender for addressing energy shortages and environmental cleanup. One of the best semiconducting photocatalysts used in wastewater treatment, disinfection, and energy evolution is graphitic carbon nitrate (g-$C_3N_4$). Researchers have used carbon quantum dots (CQDs) to maximize and enhance the photocatalytic activity of g-$C_3N_4$ and to get over the material's limits due to photoinduced charges, partial surface area, and insufficient light-capturing difficulties. In this context, the fundamentals of CQDs and g-$C_3N_4$ are described in length, along with their structural state, synthesis, and modification techniques. The classification, manufacturing procedure, and characterization of CQDs/g-$C_3N_4$ are then highlighted in this paper. Following that, it is shown how CQDs/g-$C_3N_4$ photocatalysts are used in dye removal and hydrogen evolution studies. The discussion of CQDs/g-$C_3N_4$'s present hurdles, unmet needs, and future research prospects concludes while keeping in mind their practical applications. This study shows that by embedding CQDs, the influence of charges, morphological modification, and textural quality of g-$C_3N_4$ have been altered. It is anticipated that this review will offer a practical overview and comprehension of CQDs embedded with g-$C_3N_4$ photocatalysts in order to promote their utilization. The ultimate goal of this review may be to impart a fundamental understanding of photocatalysis while also providing an expository evaluation of the most recent advancements in g-$C_3N_4$/CQDs photocatalysts in the sectors of energy and environmental security.

## 1. Introduction

Currently, environmental remediation and energy security have emerged as serious problems that are harmful to both people and the environment. Physical, chemical, biological, advanced and hybrid technologies are successfully applied to overcome energy and environmental issues [1,2]. Numerous advanced oxidation processes (AOPs) are used in wastewater treatment, including fenton oxidation, ultrasonic oxidation, moist air oxidation, photochemical oxidation, ozonation, and electrochemical oxidation [2,3]. However, there are many underlying factors that limits the application and performance of the methods such as pH dependent, costly, slow process, secondary sludge and well catalyst requires [3–5]. Consequently, researchers introduced AOPs based photocatalysis method to combat and purify the wastewater and simultaneously convert solar energy into green hydrogen [6]. Several photocatalysts such as $TiO_2$, ZnO, $Mn_2O_3$, ZnS, $SnO_2$, $Fe_2O_3$, $WO_3$ are commonly used in photocatalysis system that are widely functional in hydrogen ($H_2$) production, pollutants photodegradation, $CO_2$ reduction, and other related fields [7–15]. Therefore, conventional photocatalyst has some drawbacks such as low photo quantum efficiencies, high electron recombination rate, low efficiencies and poor stabilities that need to be solved [6,16]. A well functional photocatalyst should have an appropriate bandgap that satisfies efficient light absorption as well as an excellent conduction band (CB) and valance band (VB) and high

* Corresponding author at: Faculty of Civil Engineering Technology, Universiti Malaysia Pahang Al-Sultan Abdullah, 26300 Gambang, Pahang, Malaysia.
*E-mail address:* azrinaaziz@umpsa.edu.my (A. Abd Aziz).

https://doi.org/10.1016/j.jwpe.2023.104645
Received 22 August 2023; Received in revised form 4 October 2023; Accepted 30 November 2023

photogenerated electron and hole separation/transfer efficiency.

Since, g-$C_3N_4$ is discovered as promising nontoxic and metal free semiconductor photocatalyst that is rapidly applied in dye wastewater purification as well as hydrogen evolution [6,17]. In comparison to other semiconductor, g-$C_3N_4$ offers strong fluorescent properties such as photostability, wide excitation spectra and tuneable photo-luminescent emission spectra [18–23]. The outstanding photocatalytic performance of g-$C_3N_4$ in water splitting mechanism under visible light irradiation was initially reported by Wang et al. [24] in 2009. Momentous interest has been shown in this prospective metal-free g-$C_3N_4$ photocatalyst because of easy synthesis, high levels of physical and chemical stability, visible light induced band gap and plentiful in nature [17,18,25,26]. More importantly, g-$C_3N_4$ can be easily fabricated by thermal polymerization of abundant nitrogen-rich precursors such as urea, melamine, thiourea, cyanamide, dicyandiamide, and ammonium thiocyanate [27–31]. High levels of polymerization and the tri-*s*-triazine ring structure of g-$C_3N_4$ possesses the excellent heat and chemical resistance nevertheless suitable bandgap and CB, 2.7 eV and 1.07 eV, respectively [32]. But unfortunately, photogenerated charge carriers recombine at a rapid rate due to weak van der Waals interactions between adjacent carbon nitrate layers, high exciton binding energy, small specific area, low quantum efficiency, high electron hole and unstable in solar light [33–35]. Several modified strategies of have been developed to enhance the photocatalytic performance of g-$C_3N_4$ such as morphology control, modification with co-catalyst, coupling with other photocatalyst and doping with metal and non-metal elements, modification by carbonaceous nanomaterials [6,36]. For example, g-$C_3N_4$ is coupled with $SnO_2$ [9], $ZrO_2$ [28], $CoFe_2O_4$ [20], ZnO [12], CdS [37], BiOBr [38] and $W_{18}O_{49}$ nanowires [39] but the ultimate result does not meet the expectation as achieved by coupled with CQDs [40–42]. Thus, g-$C_3N_4$ exposed better performance and photocatalytic activity by increasing the electron transfer and reservoir properties by coupling with CQDs [6,30,43–45]. CQDs are a fascinating class of zero-dimensional carbon nanomaterials with an average size <10 nm with exceptional physicochemical, electrical, and optical properties [46]. In addition, CQDs exhibit the anticipated advantages of high surface area, aqueous stability, low toxicity, and highly tuneable photoluminescence behaviour [47]. The photocatalytic activity and visible light absorption rate of CQDs has been enhanced and improved by coupling with different semiconductor photocatalysts [47–49]. Therefore, CQDs are auspicious nanomaterials in the field of photocatalysis, wastewater treatment and energy evolution [13]. As a result, CQDs have been used as an effective part of photocatalyst design.

In this regard, a modification strategy of g-$C_3N_4$ semiconductors using CQDs was implemented to improve their adsorption, electron-hole pair migration and separation efficiency, ultra-high specific surface area and photocatalytic activity. A growing body of research has attempted to combine g-$C_3N_4$ with CQDs to develop a new photocatalyst in order to enhance their photocatalytic activity, taking into account the outstanding and distinctive features. For example, Methyl Blue (MB) and Rhodamine B (RhB) dyes were completely degreed by using CQDs modified g-$C_3N_4$ photocatalyst, simultaneously hydrogen evolution rate was outstanding [6]. Although, CQDs and g-$C_3N_4$ both are non-metal, non-toxic and their internal electrical mechanism in highly potential for the separation of photoexcited electron and hole pairs. In addition, this composite photocatalyst can produce highly active species, oxidizing free radicals thus converting them into water and treated product. However, g-$C_3N_4$ not only modifying and coupling by CQDs but also by graphene quantum dots (GQDs), N-CQDs, S-CQDs, Pt-CQDs and applied in different sectors as designated in Fig. 1.

Research on photocatalytic dye wastewater purification and hydrogen evolution through CQDs modified g-$C_3N_4$ photocatalyst have been increasing over the years. However, some of the published review articles only addressed photocatalytic activity, some of them hydrogen evolution and some of them are focusing pollutant removal separately [13,14,48]. Therefore, a comprehensive summary of CQDs modified g-$C_3N_4$ based photocatalyst for dye wastewater treatment simultaneously hydrogen evolution is required that offers an updated progress. The aim of this review is to condense the recent progress of CQDs modified g-$C_3N_4$ photocatalyst in associated with fundamentals, synthesis process, structure, properties with the application and performance in dye removal and hydrogen evolution. In Section 2, recent studies are summarized by assessing the fundamentals, synthesize, structure, application and mechanism of g-$C_3N_4$. Subsequently, the fundamentals, properties, fabrication and application of CQDs is discussed in Section 3. Classification, synthesize process and characterization of g-$C_3N_4$/CQDs photocatalysts is addressed in Section 4, followed by the mechanism of dye wastewater purification synchronously hydrogen evolution is herein discussed. The performance of g-$C_3N_4$/CQDs photocatalysts in photocatalytic dye wastewater treatment and hydrogen evolution is displays in a tabular form. After carefully analysis of the previous published research articles, there hasn't been a comprehensive review which is addressed both dye wastewater treatment and hydrogen evolution together. In Section 5, the photocatalytic performance of g-$C_3N_4$/CQDs is described by considering social, economic and environmental sustainability through SWOT analysis. Recent observations, growth, prospects, challenges and future perspectives of CQDs modified g-$C_3N_4$ photocatalyst are discussed in Section 6.

Finally, future research advances and expectations for g-$C_3N_4$/CQDs heterogeneous photocatalysts are presented in a constructive way. This study will be providing a valuable overview and insight for the promotion of applications of CQDs modified g-$C_3N_4$ based-photocatalysts.

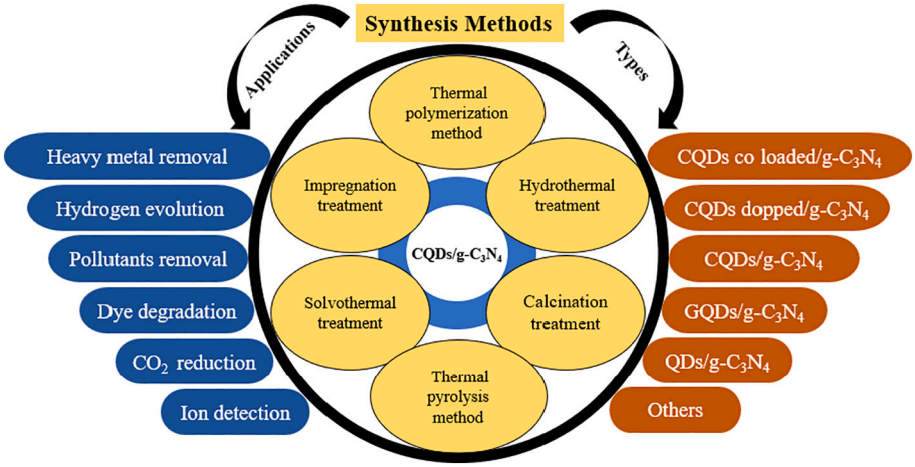


**Fig. 1.** Compendium illustration of the types, synthesis methods, and applications of CQDs/g-$C_3N_4$ photocatalysts.

In addition, offers direction and guideline for young researchers to improve the photocatalytic performance of CQDs modify g-$C_3N_4$, not only in dye wastewater treatment and hydrogen evolution but also medical, bio sensing, biotechnology sectors and so on. This research is the evidence of CQDs embedded g-$C_3N_4$ photocatalyst fabrication and its importance in the field of energy and environmental sustainability. This research might support the development of highly effective g-$C_3N_4$/CQDs photocatalyst and their commercial use.

## 2. Fundamentals of g-$C_3N_4$ photocatalyst

g-$C_3N_4$ is a promising semiconductor due to its excellent characteristic such as metal-free, lightweight and highly stable in ambient conditions [50]. This semiconductor can be applied a variety of photocatalytic applications such as $H_2$ and $O_2$ evolution, solar cell application, air purification, biomedical, and ammonia synthesis [50–52]. Recently, g-$C_3N_4$ has gained more attention as a non-metallic and visible-light activated photocatalyst and talented material for a variety of environmental remediation applications like degrading pollutants in water and wastewater [53]. Fig. 2 shows the application and controlled fabrication of g-$C_3N_4$.

Subsequently, g-$C_3N_4$ has exceptional properties due to its structural condition. For instant, g-$C_3N_4$ can work in a variety of situations due to its narrow bandgap, physical-chemical-thermal stability, effective visible-light absorption, strong optical characteristics [51,54]. And it is feasible to combine with other materials due to the amino group and triazine ring on the surface. g-$C_3N_4$ is the most stable carbon nitride phase under ambient temperature, with a two-dimensional layered allotrope comparable to graphite. As a result, when compared to other materials, carbon has the biggest number of documented allotropes. These include graphene, buckminsterfullerene, carbon nanotubes, and many more [55]. g-$C_3N_4$ is made up of *s*-triazine or tri-*s*-triazine units that are connected together using tertiary amines to produce a π-conjugation system [53]. The structure of g-$C_3N_4$ is relatively flexible, which aids doping with various elements and makes it more compatible and efficient. g-$C_3N_4$ is the most effective photocatalyst for photodegradation of carbon-based contaminants due to the features described above. Fig. 3 shows the structure and Fig. 4 bandgap position of g-$C_3N_4$.

Yet, pure g-$C_3N_4$ has a number of drawbacks, including a low efficiency in visible-light, a high electron hole recombination rate, delayed charge transport, low quantum yield, and lower charge conductivity, ineffective visible-light absorption (below 460 nm), and a small surface area [33,34]. To regulate these limits, various procedures are used, such as heteroatom doping in the bulk form of g-$C_3N_4$ to establish an impurity level in its forbidden band, which restricted its bandgap energy for visible light absorption. It has stated that the design of g-$C_3N_4$ is based on surface area, morphology, reactive sites, abundance, size, and most importantly prolonged light absorption capability. Recently, g-$C_3N_4$ energy gap engineering by metal and non-metal doping has shown to be quite beneficial in terms of regulating light acquisition ability, modifying redox band potentials, and changing luminescent and electrical features [51]. The photogenerated electron-hole pairs can explain the g-$C_3N_4$ photocatalytic mechanism under adequate light irradiation. The generation of reactive oxygen species (ROS) and overall electron transport is depicted in Eqs. (1)–(4) [57].

$$g - C_3N_4 + \text{light} \rightarrow g - C_3N_4\ (h^+ - e^-) \quad (1)$$

$$g - C_3N_4\ (e^-) + O_2 \rightarrow g - C_3N_4 + \dot{O}_2^- \quad (2)$$

$$2\ g - C_3N_4\ (e^-) + O_2 + 2\ h^+ \rightarrow 2\ g - C_3N_4 + H_2O_2 \quad (3)$$

$$H_2O_2 + g - C_3N_4\ (e^-) \rightarrow g - C_3N_4 + \dot{O}H + OH^- \quad (4)$$

Three phases are involved in the photocatalytic process on g-$C_3N_4$. Firstly, electrons on the VB of g-$C_3N_4$ are energised, jump to the CB and VB is left with positive holes when exposed to light. The divided electrons and holes then travel to photocatalyst surfaces, where they initiate redox processes. Dissolved oxygen and $H_2O/OH^-$ can operate as electron acceptors and donors, respectively, in aqueous solutions. Finally, the produced superoxide anion ($O_2$) and hydroxyl radical (•OH) have the ability to mineralize organic contaminants and convert them to innocuous chemicals [58]. Table 1 shows the general information regarding crystallite size, surface area, band gap and visible-light degradation rate of g-$C_3N_4$.

g-$C_3N_4$ is cost effective due to it is synthesized from numerous low-cost nitrogen precursors e.g., melamine, urea, cyanamide, thiourea and dicyandiamide [25,29,48,59,60] as displays in Fig. 5. g-$C_3N_4$ photocatalyst has been prepared by using a variety of physical and chemical methods. The top down and bottom-up techniques have widely been accepted. Breaking up larger g-$C_3N_4$ blocks into smaller units, such as g-$C_3N_4$ nanosheets, is part of the top-down method. On the other hand, smaller molecules are incorporated into bigger complex compounds via a bottom-up strategy. In addition, sol-gel process, thermal polymerization, solvothermal technique, precipitation, hydrothermal, template assisted techniques were frequently used for the synthesis of g-$C_3N_4$ photocatalyst [27,61,62]. There have been numerous attempts to produce the necessary g-$C_3N_4$, where doping has been deemed to be the most effective method. The choice of precursor and synthesis process is crucial for obtaining the desired properties (physical and chemical) in nanohybrids.

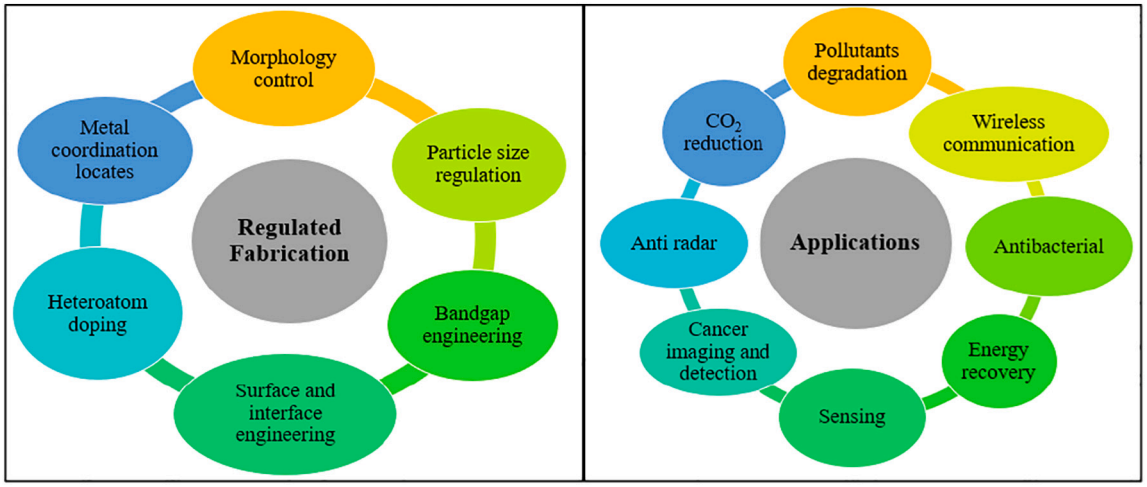


**Fig. 2.** Potential applications and modulations of g-$C_3N_4$.

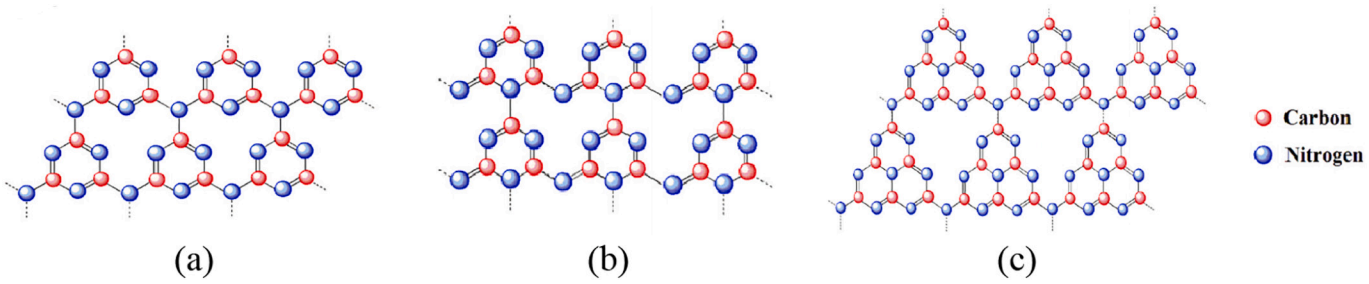


**Fig. 3.** Structure of g-$C_3N_4$ (a) s-tris-azine based hexagonal structure, (b) *s*-triazine based orthorhombic structure, (c) tri-*s*-triazine-based structure [56].

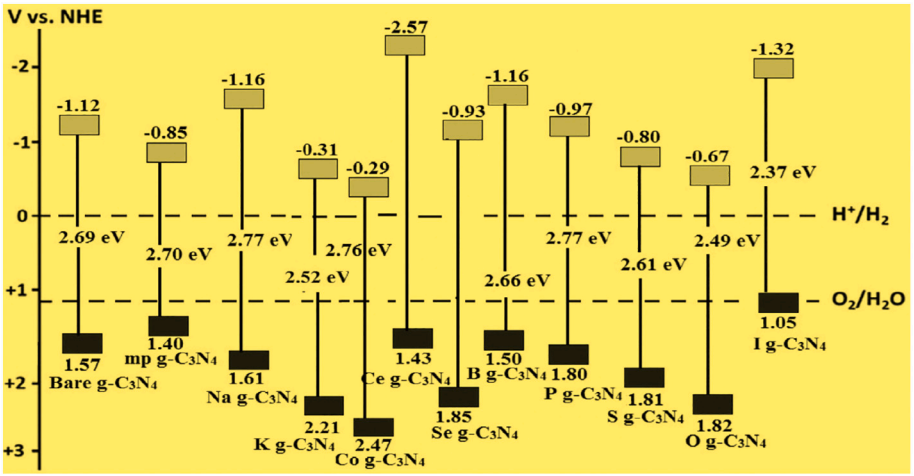


**Fig. 4.** Band gap positions of pure g-$C_3N_4$ and doped g-$C_3N_4$ [52].

**Table 1**
Crystallite size, surface area, band gap and visible-light degradation rate of g-$C_3N_4$ derived from different precursors [58].

| Precursor composition | Surface area ($m^2g^{-1}$) | Crystallite size (nm) | Band gap (eV) | Rate constant for Acid Orange (AO) 7 (k) ($min^{-1}$) |
|---|---|---|---|---|
| Melamine | 11.24 | 9.18 | 2.58 | 0.034 |
| Urea | 55.10 | 8.39 | 2.69 | 0.257 |
| Melamine and urea | 18.54 | 10.02 | 2.54 | 0.118 |
| Thiourea | 13.10 | 8.81 | 2.61 | 0.009 |
| Thiourea and urea | 24.35 | 9.67 | 2.77 | 0.196 |
| Melamine and urea and thiourea | 16.48 | 9.61 | 2.64 | 0.043 |
| Melamine and thiourea | 9.42 | 9.36 | 2.60 | 0.030 |

An improved highly thermal polymerization treatment method was applied for the synthesize of g-$C_3N_4$ through melamine as a precursor by Feng et al. [48]. A certain amount of melamine was kept into an alumina crucible with proper cover and nonstop heated at 550 °C for 4 h with a heat rate of 55 °C/min in a furnace. The resultant sample kept to cool under room temperature and found bulk yellow colour product that apprised as g-$C_3N_4$ (Fig. 6a). Same precursor has been considered by several researchers for fabrication of g-$C_3N_4$ photocatalyst under different temperature and duration [59,60,63,64]. g-$C_3N_4$ was synthesized by using thiourea as a precursor with a continuous heat at 550 °C for 2 h in a muffle furnace with a heating rate of 5 °C/min [46]. Finally, subsequent yellow colour product is obtained as g-$C_3N_4$ (Fig. 6b). A simple thermal heating technique was conducted by Hak et al. [65] to synthesize the g-$C_3N_4$ by urea as a precursor. Initially, urea was kept in a crucible with suitable cover and heat at 80 °C for 12 h in an oven. Thereafter, the crucible was entered into a muffle furnace and seated at 550 °C for 3 h towards further heat with a heating ramp of 10 °C/min. The resulting yellow colour outcome was then rinsed with nitric acid and distilled water. At the end of the process, the wet sample was centrifugation for 10 min at 3500 rpm to remove unwanted residual and dried at 80 °C overnight to obtain pure g-$C_3N_4$ (Fig. 6c). Several studies have developed g-$C_3N_4$ using the same precursor but at various heating rates and duration [6,17,23,44,59,61,66].

Thermal decomposition treatment was executed to synthesize g-$C_3N_4$ through dicyandiamide as a precursor. Certain amount of dicyandiamide was placed in a crucible and loaded into a muffle furnace for uninterrupted heating at 450 °C for 2 h with a heating ramp 2 °C/min followed by maintaining additional heat for 4 h at 550 °C [35]. Subsequently, the substance was cooled under room temperature, washed properly with distilled water and filtered to eliminate undesirable ingredients. Finally, the sample was placed inside an oven and heat at 100 °C to obtain dry g-$C_3N_4$ powder (Fig. 6d). The synthesis of g-$C_3N_4$ through same precursor utilizing varied temperatures and period of time has been investigated in numerous research [59,60,67]. g-$C_3N_4$ was fabricated through a thermal heating process by using cyanamide as a precursor. Cyanamide was placed in a crucible with good cover and loaded into a muffle furnace for constant heat at 500 °C for 4 h, followed by continuing further heat for 2 h at 520 °C with a heating ramp 20 °C/min [60]. Lastly, the crucible was cooled under room temperature and the obtained yellow colour sample is considered as cyanamide induced g-$C_3N_4$ (Fig. 6e).

However, researchers also applied two or more precursors to synthesize the non-metal g-$C_3N_4$ photocatalyst. g-$C_3N_4$ was prepared by Shi et al. [31] through the mixture of melamine and urea as a precursor under thermal heating process. A specific quantity of melamine and urea were mixed properly by grinding in a certain period. Subsequently, the

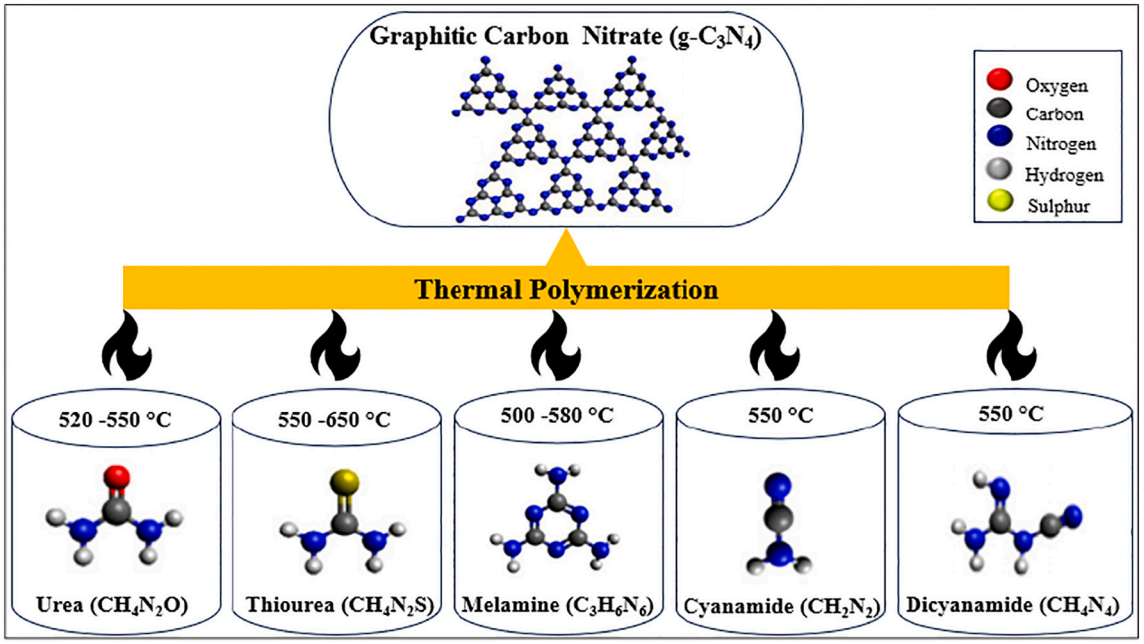


**Fig. 5.** Development and synthesis process of g-$C_3N_4$ through thermal polymerization.

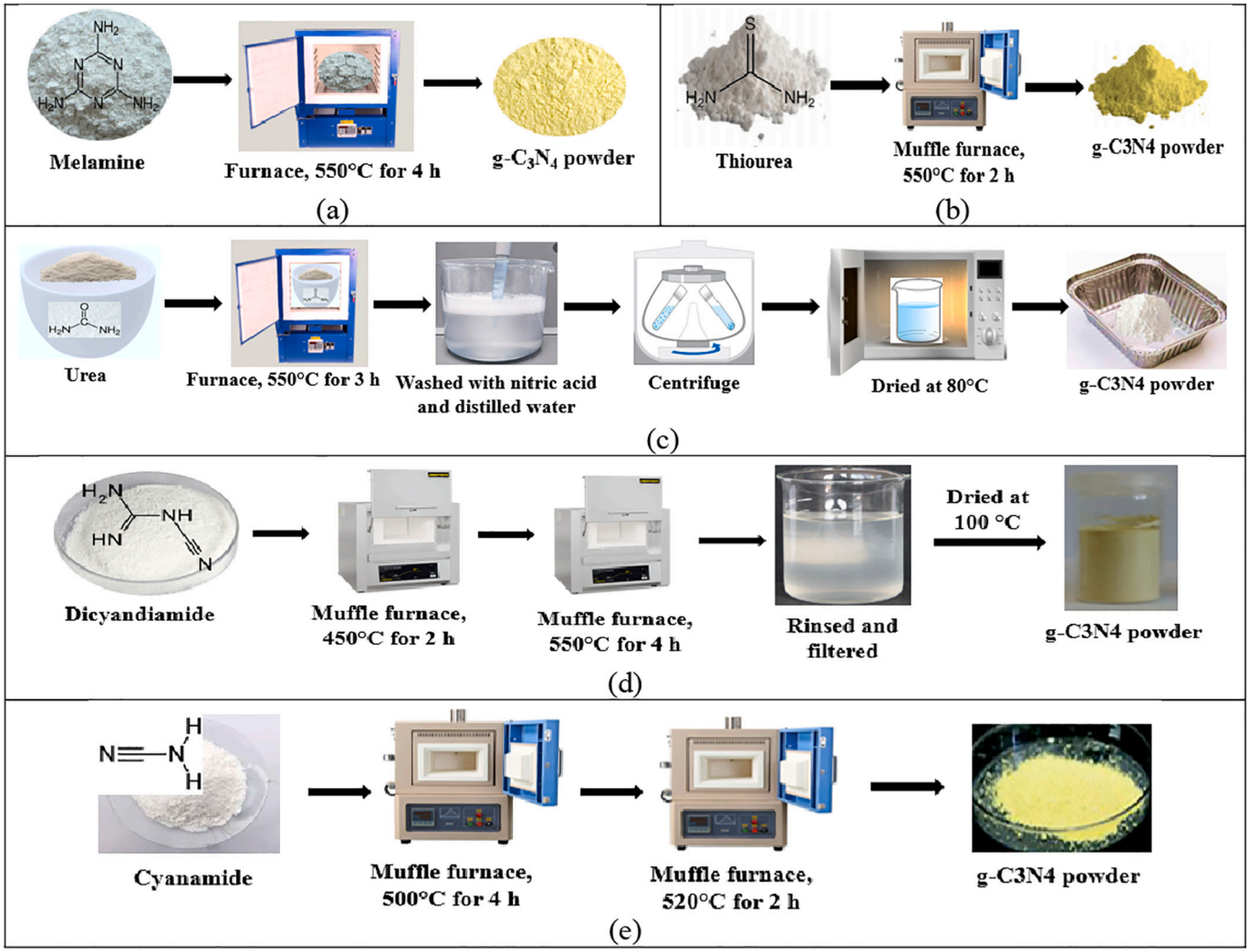


**Fig. 6.** Synthesis of g-$C_3N_4$ from (a) Melamine; (b) Thiourea; (c) Urea; (d) Dicyandiamide; (e) Cyanimide.

mixture is placed in an alumina crucible and continuous heat at 550 °C for 4 h with a heating ramp 2.3 °C/min. Finally, the obtained yellow colour powder sample is found as g-$C_3N_4$ photocatalyst. Furthermore, the same precursors were applied by Xu et al. [68] to synthesize the g-$C_3N_4$ with diverse duration and temperature. A combination of urea and thiourea was polymerized for 2 h at 550 °C with a heating ramp rate of 3 °C to fabricate g-$C_3N_4$ [69]. On the other hand, Yao et al. [67] synthesized g-$C_3N_4$ by utilizing the mixture of dicyandiamide and urea. The

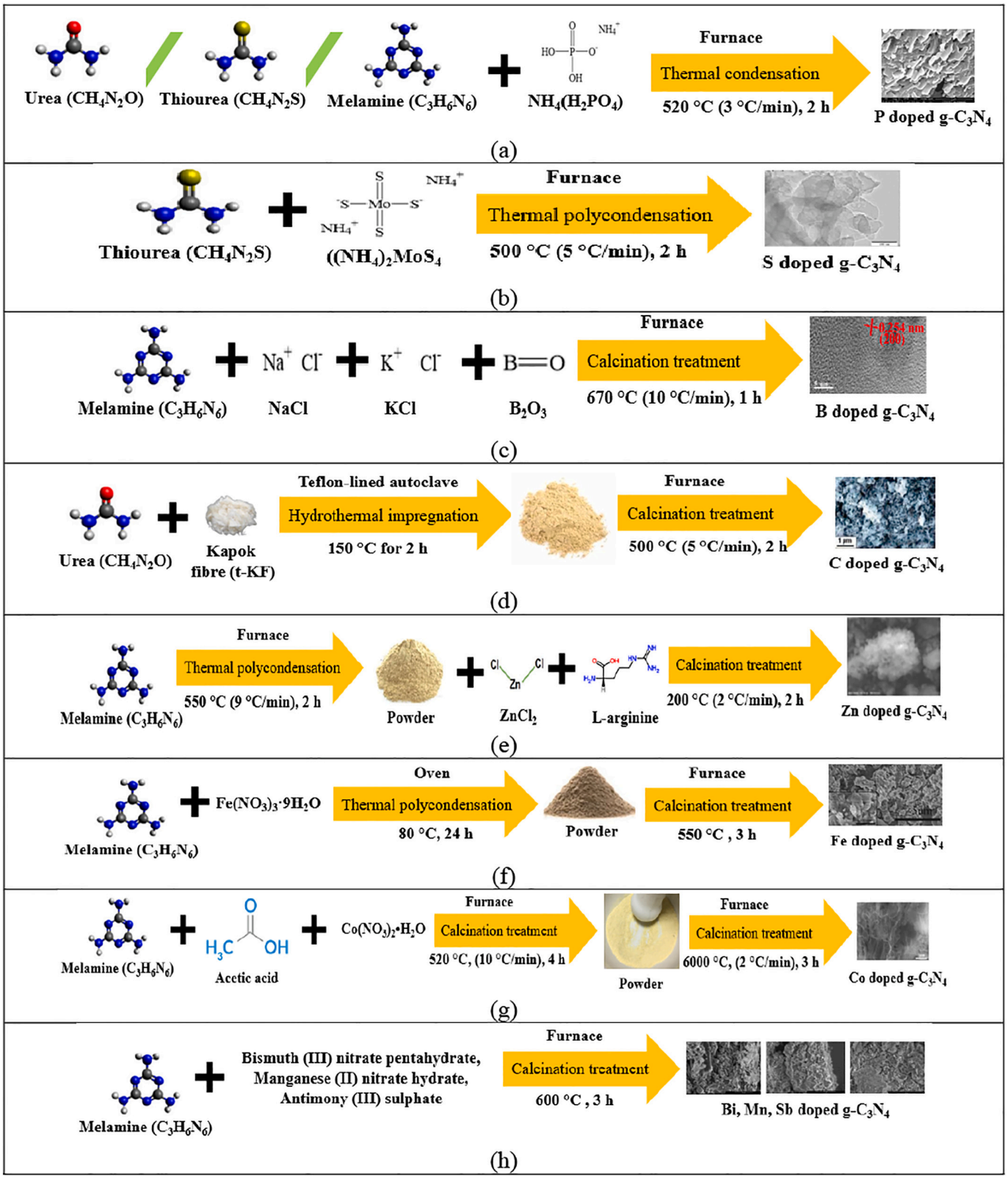


**Fig. 7.** Synthesis routes for the preparation of non-metal (a) Phosphorous (P) [25]; (b) Sulphur (S) [73]; (c) Boron (B) [74]; (d) Carbon (C) [75] and metal (e) Zink (Zn) [76]; (f) Iron (Fe) [77]; (g) Cobalt (Co) [78]; (h) Bismuth (Bi), Manganese (Mn), Antimony (Sb) [79] doped g-$C_3N_4$.

mixture was then nonstop heated at 550 °C for 4 h, followed by keeping the heat at 500 °C for additional 2 h to obtain the yellow colour substance considered as g-$C_3N_4$.

Although, a number of techniques have been established for the fabrication of nanocomposites based on g-$C_3N_4$. The preparation of g-$C_3N_4$ based catalysts can be split into three categories: (i) physical (physical vapor deposition, ultrasonic treatment, chemical vapor condensation, solid state reaction, gas condensation), (ii) chemical (template, thermal polymerization, microwave-assisted heating, pyrolysis, sol-gel, hydrothermal/solvothermal method) and (iii) mechanical synthesis methods (mechanical grinding) [56,70]. Physical procedures do not disrupt the crystal lattice structure of g-$C_3N_4$, but they are hardly used in practical production because of the necessity for high-purity raw materials and specialised equipment [71]. It has been discovered by the scientific community that doped g-$C_3N_4$ is more effective than pure g-$C_3N_4$ [23,44,72] (Fig. 7).

Based on the above discussion, it can be summarized that the precursor has a significant importance in the quality and performance of g-$C_3N_4$. The precursors have the potentiality to enhance the morphology and optical properties of any composites in conjunction with g-$C_3N_4$ [48]. That particularly improve the application and overall performance of the particular composite photocatalyst. Among the various precursors of g-$C_3N_4$, urea possess optimum quality and highly efficiency in the field of pollutants removal and energy evolution [6,65]. In addition, as a precursors urea is cheap, abundant and has the capability to prepare more effective composite photocatalyst modifying with various biological and chemical synthesized CQDs [80]. On the other hand, some precursors of g-$C_3N_4$ need to be rinsed with acid and distilled water prior to use or combined with other photocatalyst due to the removal of any unwanted particles, residual and impurities [65].

## 3. Fundamentals of CQDs photocatalyst

CQDs are a novel form of 0-dimensional carbon material with a size <10 nm [81,82]. CQDs are made up of discrete nanoparticles and quasi-spherical particles with layered of graphene-based structures. Researchers from a different fields have used CQDs for a variety of purposes such as biomedical and biotechnological applications, dye-synthesized solar cells, light-emitting devices, imaging and bio-imaging, electrochemical studies, semiconductor devices, chemical sensing, photo-catalysing, and electrocatalysis [81,83–88]. CQDs have gotten a promising attention in several applications, particularly in wastewater treatment. Because of its effective characteristics such as low toxicity, high dispersibility of water, low-cost manufacturing, stable Photoluminescence (PL), superior chemical stability, outstanding photostability and electron reservoir features [81,82,89]. Due to quantum confinement effect and optical stability qualities, CQDs provide a good photoluminescent signal, strong fluorescence activity, chemical inertness, and durability [81]. In energy conversion applications, CQDs can be used as a substitute for semiconductor quantum dots. The properties of CQDs are depicted in Fig. 8a.

CQDs are a type of conjugated π structure material that is made up of amorphous to nanocrystalline graphite carbon or graphene [44]. CQDs have excellent electron transport and storage capabilities. CQDs also have outstanding PL capabilities for both up and down conversion, as well as strong electrical and optical functionality [44,82]. The conjugated π-domains and PL emission related with the surface state, conjugated structures, and specific structure locations are credited with CQDs capacity to fully use the sunshine spectrum. Furthermore, CQDs can transform long-wavelength into short-wavelength because of having various nanoparticle sizes and emissive trap states on the CQD surface [86]. The carbon precursors emissivity used as raw materials also affect the luminous properties of CQDs [90]. Fig. 8b depicts the fundamental distinctions between CQD surface functionalization and passivation procedures.

CQDs can be synthesized via breaking bulk carbon structures and the chemical reactions of precursors. This process is conducted under two main methods named top-down and bottom-up approach. However, there are five sub approaches are commonly considered under both approaches. For example, the top-down methods are laser ablation, arc discharge, electrochemical oxidation, ultrasonic treatment, chemical ablation and bottom-up approaches are hydrothermal, template method, plasma treatment, thermal decomposition and microwave irradiation techniques. Among the entire synthesis approach of CQDs, hydrothermal and microwave treatments are common, facile, and widely applicable [45,91,92].

CQDs were successfully synthesized by Remli and Aziz [91] through watermelon rinds as a carbon source in a simple hydrothermal synthesis method. Watermelon rinds juice was mixed with ethanol (4:3 ratio) and stirred for a certain period for homogenous suspension. Thereafter, the mixture was transferred into a stainless-steel Teflon autoclave and continuous heating for 2.5 h at 120 °C in an oven. In order to separate the less fluorescent deposit and obtain highly fluorescent CQDs, the resulting dark brown solution is centrifuged and rinsed with dichloromethane and acetone (Fig. 9a). CQDs were synthesized by improved sonication technique by suing glucose, distilled water and sodium hydroxide solution [48]. 2 h ultrasonic treatment was applied to the combined and colourless solution. After that, HCl was used to neutralise the brownish yellow solution and further dialysis to obtain the purified CQDs solution [93] as represented in Fig. 9b. Therefore, different metal and non-metal dopes CQDs offers outstanding performance in various application by overcoming monochromatic fluorescence and less

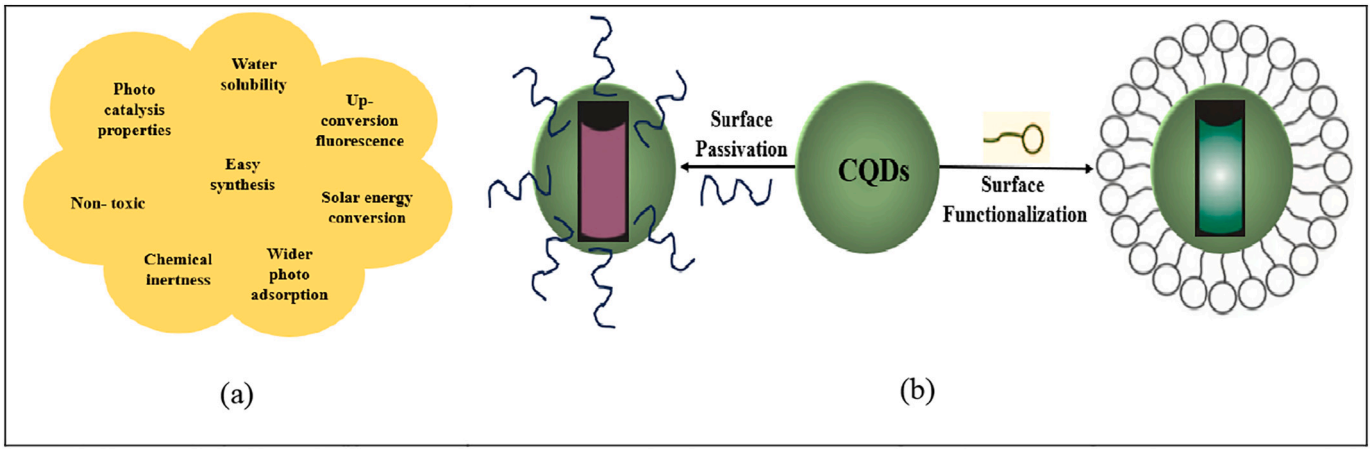


**Fig. 8.** (a) Properties, (b) Surface functionalization and passivation of CQDs [90].

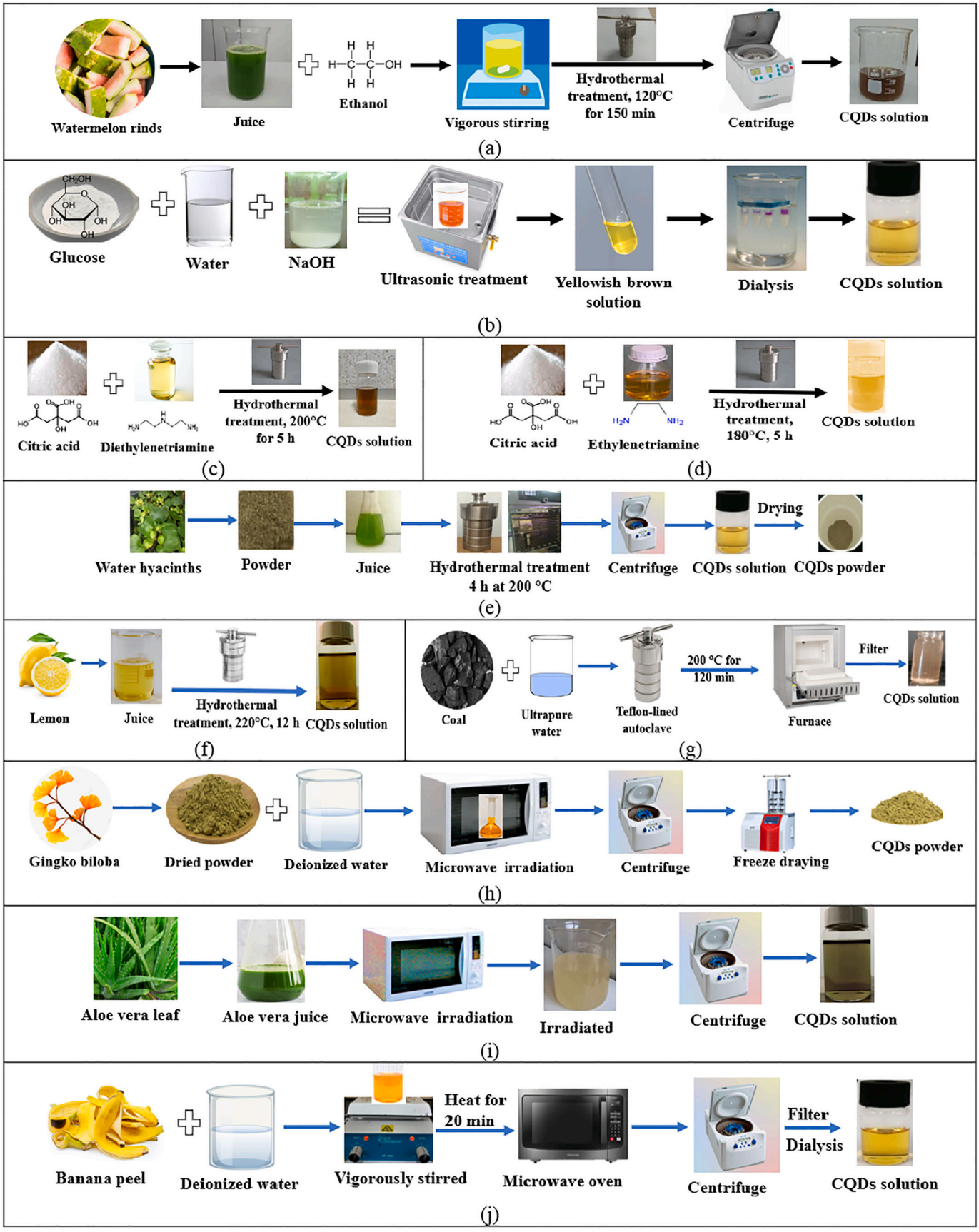


**Fig. 9.** Synthesis of CQDs from (a) watermelon rinds; (b) glucose; (c-d) citric acid; (e) water hyacinths; (f) lemon; (g) coal; (h) gingko biloba; (i) *Aloe vera* leaf; (j) banana peels.

fluorescence yield of CQDs [44,94]. Aghamali et al. [95] fabricated nitrogen doped CQDs (N-CQDs) through the hydrothermal synthesize method by using citric acid. Certain amount of citric acid and diethylenetriamine was added with distilled water and shifted to autoclave with a temperature at 200 °C in an oven for 5 h. A transparent, light-yellow solution was formed once the process completed and considered as N-CQDs (Fig. 9c). Numerous researchers applied the same precursors for the development of N-CQDs [31,44,61,96] with different dose, duration and temperature. On the other hand, Hong et al. [30] also synthesized CQDs by applying advance hydrothermal method with citric acid, distilled water and ethylenediamine solution. The solution was moved into an autoclave and constant heated for 5 h at 180 °C. The reaction was followed by a natural cooling of the autoclave to room temperature. A semi-permeable membrane was used to perform dialysis on the product in order to get the CQDs as described in Fig. 9d. Similar method and process were followed by several researchers [6,17,45,64] to synthesize CQDs, however the heating temperature and duration was different.

Fabrication and development of the CQDs by using biomass is modern innovation by researchers. Hak et al. [65] formed CQDs by facile hydrothermal technique through dried water hyacinths leaves. The mixture of distilled and water hyacinths leaves powder were vigorously stirred to make the homogenous solution. Later on, the solution was shifted into an autoclave for continuous heating at 200 °C for 4 h in the oven. The autoclave was cooled at room temperature and centrifugation to remove the large particle to obtain yellowish-brown solution considered as CQDs. Finally, the solution is dried at 100 °C in an oven to secure solid form of CQDs as shows in Fig. 9e. Lemon juice was exert to synthesize CQDs with a certain volume of ethanol via hydrothermal treatment by Jin et al. [46]. The pre mixture solution was flushed into an autoclave and a continuous heated for 12 h at 200 °C in an oven to get the CQDs solution as illustrates in Fig. 9f. Lemon juice also employed to synthesize CQDs by Olmos-Moya et al. [97] through microwave assisted technique under diverse temperature and duration. Coal and distilled water were mixed to fabricate CQDs through hydrothermal treatment method by Saikia et al. [88]. Initially, the mixture was placed in a Teflon-lined autoclave reactor and later on loaded into a furnace for continuous heat for 2 h at 200 °C (Fig. 9g). After air cooling, the pH was determined and the solution was undergone for filtration with a dialysis membrane kit to preserve the CQDs.

Furthermore, CQDs have been synthesized through microwave assisted technique from dry gingko biloba as a carbon precursor by Genc et al. [92]. Certain amount of gingko biloba powder was mixed with distilled water and loaded into a domestic microwave oven at various period of time scale. Thereafter, the dark-brown mixture was centrifugated and the supernatant was collected by filtering. Finally, the supernatant was dried in a vacuum freeze to obtain powder is considered as CQDs as displayed in Fig. 9h. Another research has been conducted by Malavika et al. [98] for the preparation of CQDs from *aloe vera* leaf juice under microwave assisted synthesis process. Fresh and smashed *aloe vera* leaf was merged with deionized water and shifted to a conical flask for microwave treatment. After a certain period, the reaction is completed and sample is collected to allow cool at ambient temperature. Subsequently, the sample was centrifuged to avoid unwanted particles and contaminants. Finally, CQDs are collected by a separation method named silica gel followed by proper dialysis as exhibited in Fig. 9i. It is mentioned that CQDs were formed from the biomass by the acquired fluorescence emission under UV light [6,85,97,98]. Huang et al. [99] synthesized CQDs through the mixture of banana peels and distilled water under microwave assisted method. The pre-mix solution of banana peels and distilled water was placed to a domestic microwave oven for 20 min. The resultant solution was cooled under room temperature and centrifuge to eliminate undesired large particles. The resultant solution is filtered and dialyzed to obtain CQDs solution (Fig. 9j). Finally, the solution is lyophilized to secure the powder considered as CQDs.

## 4. Design of CQDs modified g-$C_3N_4$ photocatalyst

Although, there are some drawbacks of pure g-$C_3N_4$ such as limited surface area, poor quantum efficiency and high electron hole. These limitations are responsible to reduce the performance of g-$C_3N_4$ in various environmental applications. Numerous studies indicate that CQDs modified g-$C_3N_4$ has more photoactivity than pure g-$C_3N_4$ by encountering and improving the surface area, quantum efficiency, electron transfer and reservoir properties [6,30,31,44,52,85]. There are several classes of metal free CQDs modified g-$C_3N_4$ ternary and binary photocatalysts and significantly enhance the photocatalytic performance. There is a schematic representation of the classification of CQDs embedded g-$C_3N_4$ as displays in Fig. 10.

Presently, a number of strategies have been devised to fabricate CQDs modified g-$C_3N_4$ nanocomposites because of their momentous application for the abolition of pollutants and alternative green hydrogen energy evolution. However, the physical, chemical and optical characteristics of the modified photocatalysts are critically influenced by the synthesis techniques and conditions. For example, Li and co-workers investigated the photocatalytic efficiency of CQDs modified g-$C_3N_4$, fabricated through a direct calcination process by the combination of melamine, and cyanuric acid [100]. A certain amount of cyanuric acid was mixed with melamine and distilled water for 12 h under ardent stirring, wherever melamine and cyanuric acid have a 1:1 M ratio. Thereafter, the milky solution is vaporising in an oil bath drying oven at 90 °C. The powder was then put into an alumina crucible with a cover and heated for 4 h at 500 °C in a muffle furnace with a 2.3 °C/min. Once it has naturally cooled to ambient temperature, the obtained solid powder form is considered as CQDs modified g-$C_3N_4$ as displayed in Fig. 11a. According to this study, the pre-prepared CQDs/g-$C_3N_4$ in an exceptional multifunctional photocatalyst hydrogen evolution through water splitting and dye degradation. This research demonstrated incredibly high hydrogen evolution rate of 24,760 μmol/h/g and completely degradation of MB within 240 min. Most recently, Liu et al. [23] successfully synthesized CQDs/g-$C_3N_4$ composite through citric acid and urea under impregnation approach. The synthesized nanocomposite demonstrated superior light harvesting, a narrow band-gap, and workable electron transport capabilities, which led to increased photocatalytic activity for the degradation of RhB. Furthermore, the nanocomposite completely degraded RhB within 120 min and offered a hydrogen evolution rate of 626.93 μmol/h/g. The simultaneous operation of the oxidation and reduction processes is thought to be the cause of the improved photocatalytic efficiency and increasing the number of electrons and holes produced for redox processes as well as the effectiveness of charge carrier separation. On the other hand, Zhang et al. [6] fabricated CQDs/g-$C_3N_4$ composite through the same precursors nevertheless under the hydrothermal treatment approach. The efficiency of producing hydrogen as well as degrading MB and RhB was significantly improved by CQDs/g-$C_3N_4$ composite under visible light. The result displayed that the MB and RhB were completely degraded by 20 min and 110 min, respectively. Simultaneously, the hydrogen evolution rate was 1291 μmol/g/h under 300 W Xe lamp. However, charge transfer and separation efficiency of the $e^-/h^+$ pairs is critically increased by adding CQDs on the surface of g-$C_3N_4$.

Hak et al. [65] synthesized CQDs/g-$C_3N_4$ by the mixing of water hyacinths induced CQDs and urea induced g-$C_3N_4$ under simple hydrothermal method. Following that, the mixture was placed in a Tefon-lined autoclave and nonstop heated at 100 °C for 2 h. The autoclave then allowed to cool in room temperature and the resultant samples were rinsed with distilled water. Thereafter, the washed solution is undergone for centrifugation and the precipitate was dried at 80 °C to secure the CQDs/g-$C_3N_4$ composite as shows in Fig. 11b. Concurrently, CQDs/g-$C_3N_4$ composite has been fabricated by using thiourea tempted g-$C_3N_4$ and lemon synthesized CQDs [46]. The mixture was then effectively stirred before being put into an autoclave for continuous heat for 12 h at 220 °C in an oven. The precipitant was assembled by centrifugation and

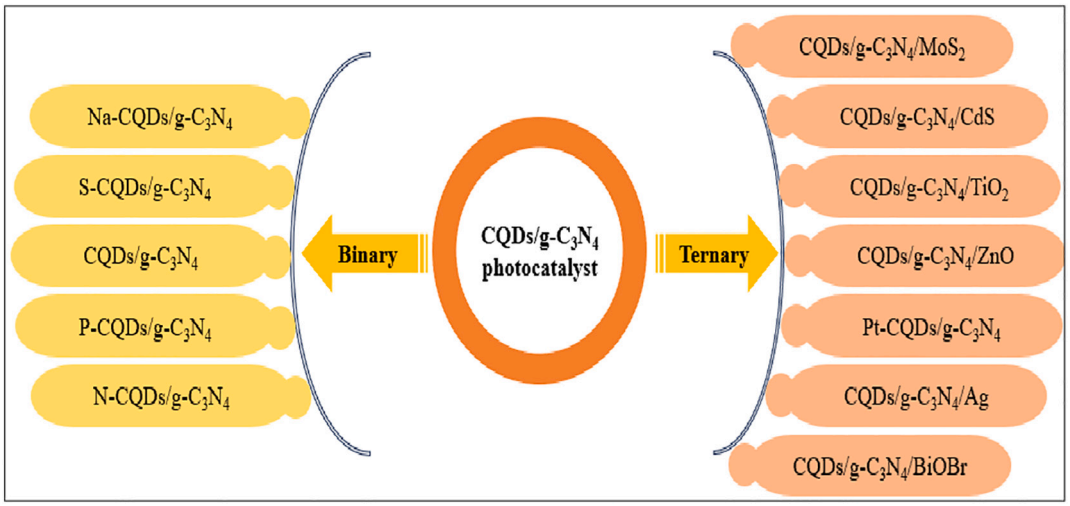


**Fig. 10.** Graphical representation of the classification of CQDs/g-$C_3N_4$ based photocatalysts.

washed with distilled water and ethanol before being dried at 60 °C in an oven. Finally, the obtained powder is considered as CQDs/g-$C_3N_4$ nanocomposite as shows in Fig. 11c. Hong and coresearchers [30] synthesized CQDs/g-$C_3N_4$ heterojunctions by low temperature method with the presence of citric acid and melamine as precursors [64]. The mixture is simply nonstop stirred for 12 h and CQDs/g-$C_3N_4$ composite was collected by drying 80 °C in an oven as expressions in Fig. 11d. Urea and citric acid induced bulk g-$C_3N_4$ and CQDs has been applied to fabricate CQDs/g-$C_3N_4$ composite [29,85]. Different volume of CQDs and g-$C_3N_4$ were merged by magnetic stirring and dried at 60 °C to obtain as powder form. Thereafter, the powder was heated for 3 h at 550 °C with a heating ramp of 15 °C/min as shows in Fig. 11e-f. Finally, the sample was collected and considered as CQDs/g-$C_3N_4$ composite. Similar precursors has been utilized by numerous researchers to synthesize noble CQDs/g-$C_3N_4$ nanocomposite [17,44,45,61,66]. Wang and coworkers [63] prepared CQDs/g-$C_3N_4$ photocatalysts through L-Ascorbic acid and melamine as precursors by simple hydrothermal technique. Certain amount of melamine induced g-$C_3N_4$ was mixed into the L-Ascorbic acid and distilled water solution by sonication and vigorously magnetic stirrer. Subsequently, the mixture was placed into a Teflon-sealed autoclave for continuous heated for 4 h 180 °C and then allowed to cool at room temperature. The sample was centrifuged and washed by distilled water and ethanol, dried at 60 °C to collect the precipitants considered CQDs/g-$C_3N_4$ composite as illustrates in Fig. 11g.

### *4.1. Characterization of CQDs-based g-C3N4 photocatalytic materials*

#### *4.1.1. Fourier transform infrared (FTIR) spectroscopy*

The functional and fingerprint group of CQDs, g-$C_3N_4$ and CQDs/g-$C_3N_4$ composite are acknowledged by FTIR spectroscopy as shows in Fig. 12. According to Hak et al. [65], an extensive and slight peak of water hyacinths leaves synthesized CQDs is noticed at 3400 $cm^{-1}$ and 2932 $cm^{-1}$ that attributable to the stretching vibration mode of O—H and C—H, respectively (Fig. 12a). However, outstretched carbonyl groups of C═O is confirmed due to 1616 $cm^{-1}$ band and vibrational band peaks (1052 $cm^{-1}$ and 1112 $cm^{-1}$) is correspondent to C–O–C vibrations stretching. On the other hand, urea synthesized g-$C_3N_4$ offers numerous absorption peaks at 1241 $cm^{-1}$ and 1630 $cm^{-1}$ that dispensed to C—N ($sp^3$) and C═N ($sp^2$) stretching that matches with the typical stretching modes of the CN heterocycles. Thus, the triazine breathing mode of g-$C_3N_4$ was attributed to the strong peak at 808 $cm^{-1}$. When CQDs is merged with g-$C_3N_4$, the intensity of these distinctive bands is reduced in all composites that is may be due to low doses of CQDs as shows in Fig. 12a. The frail CQDs absorptions peak was obscured by the robust g-$C_3N_4$ absorptions peak. As CQDs dose is increased by 40 wt%, the stretching mode of CN heterocycles shows a little blue-shift from 1241 $cm^{-1}$ to 1238 $cm^{-1}$ (Fig. 12a) that is due to reaction between CQDs and g-$C_3N_4$. Li and peers [85] synthesized CQDs/g-$C_3N_4$ photocatalyst by using urea and citric acid as carbon precursor where N—H group is shown by the large band at 3000–3400 $cm^{-1}$ (Fig. 12b). In contrast, the O—H band is caused by surface-adsorbed hydroxyl groups and uncondensed amino groups. Peaks at 1200–1600 $cm^{-1}$ and 807 $cm^{-1}$ are associated with the triazine unit stretching and breathing modes, respectively [23,100]. It can be can infer that the initial g-$C_3N_4$ structure was not materially reformed by the addition of a slight quantity of CQDs. Consequently, L-ascorbic acid and melamine synthesized CQDs, g-$C_3N_4$ and CQDs/g-$C_3N_4$ photocatalyst by Wang et al. [63] shows outstanding functional group through FTIR. The position of the primary distinguishing absorption peaks of CQDs at 786, 1023, 1384, 1621, 1704, 2868, 2970, and 3419 $cm^{-1}$ which allocated the functional groups of C—O, C—O, -$CH_3$, C═C, C═O, -$CH_2$, -$CH_3$ and –OH as shows in Fig. 12c. Different absorption peaks are associated with the functional groups of the tri-*s*-triazine structure (808 $cm^{-1}$), heptazine heterocycles (1635 $cm^{-1}$, 1410 $cm^{-1}$, and 1242 $cm^{-1}$) and the unreacted amino group (3100 $cm^{-1}$ - 3300 $cm^{-1}$) in g-$C_3N_4$. Interestingly, CQDs/g-$C_3N_4$ photocatalyst also offers the similar spectrum with g-$C_3N_4$ because of low dose of CQDs on the surface of g-$C_3N_4$ and the intersection of peak positions [85,101]. Several functional groups including OH, CH, NH, C═C, C═O, C—H, O—H, C—O reflecting the abundance of carboxyls, hydroxyls, and amines functions [23,96].

#### *4.1.2. Transmission electron microscopy/high regulation TEM (TEM/HRTEM)*

Internal structure of CQDs, g-$C_3N_4$ and CQDs/g-$C_3N_4$ nanocomposite, their size distribution and morphology can be described by TEM. Citric acid induced CQDs offers a homogenous distributed circular shape with a size of 4 nm in TEM image [29] as displays in Fig. 13A1. TEM of Ethylenediaminetetraacetic acid synthesized pure CQDs offers a size of 5–10 nm that are well diversified (Fig. 13A2) [102]. However, the size of citric acid synthesized CQDs are around 10 nm [66] as shows in Fig. 13A3, that may be due to the CQDs solution not having undergone proper filtering. On the other hand, citric acid synthesized CQDs offers a well distributed carbon dots with average size of 5 nm. In addition, the lattice gap of a single CQDs particle in the HRTEM image is approximately 0.21 nm (Fig. 13A4) [31]. Alike, TEM image of citric acid synthesized CQDs displays a uniform distribution of carbon dots primarily in sizes between 2 and 5 nm (Fig. 13A5) [6]. So, the size of CQDs and their distribution can be varied not only for precursors but also synthesis duration, temperature, environment and methods. TEM image of g-$C_3N_4$ offers several tremendously folded paper sheet with micron in size as

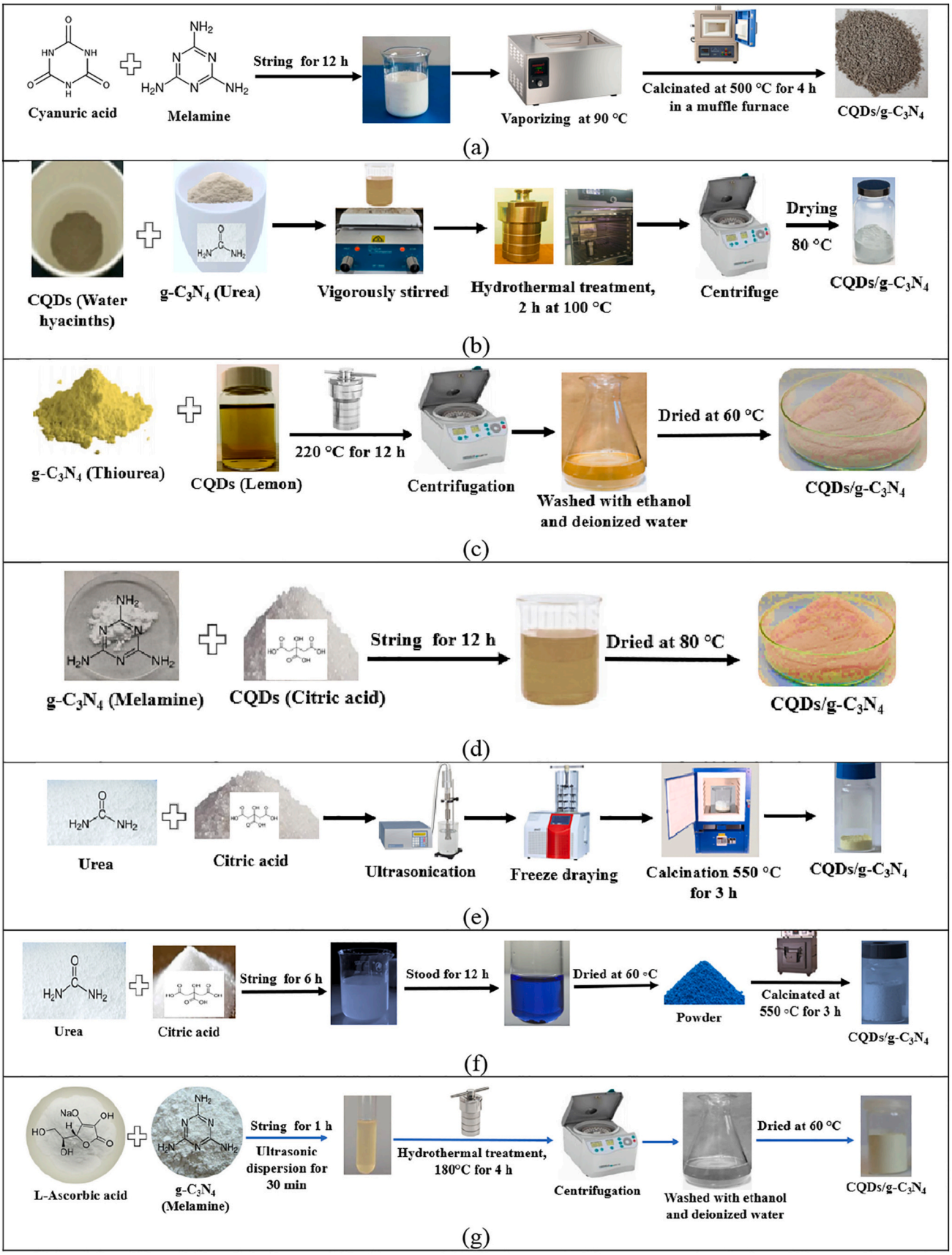


**Fig. 11.** Synthesis of CQDs/g-$C_3N_4$ composite from (a) cyanuric acid and melamine; (b) water hyacinths and urea; (c) lemon and thiourea; (d) melamine and citric acid; (e-f) urea and citric acid; and (g) L-ascorbic acid and melamine.

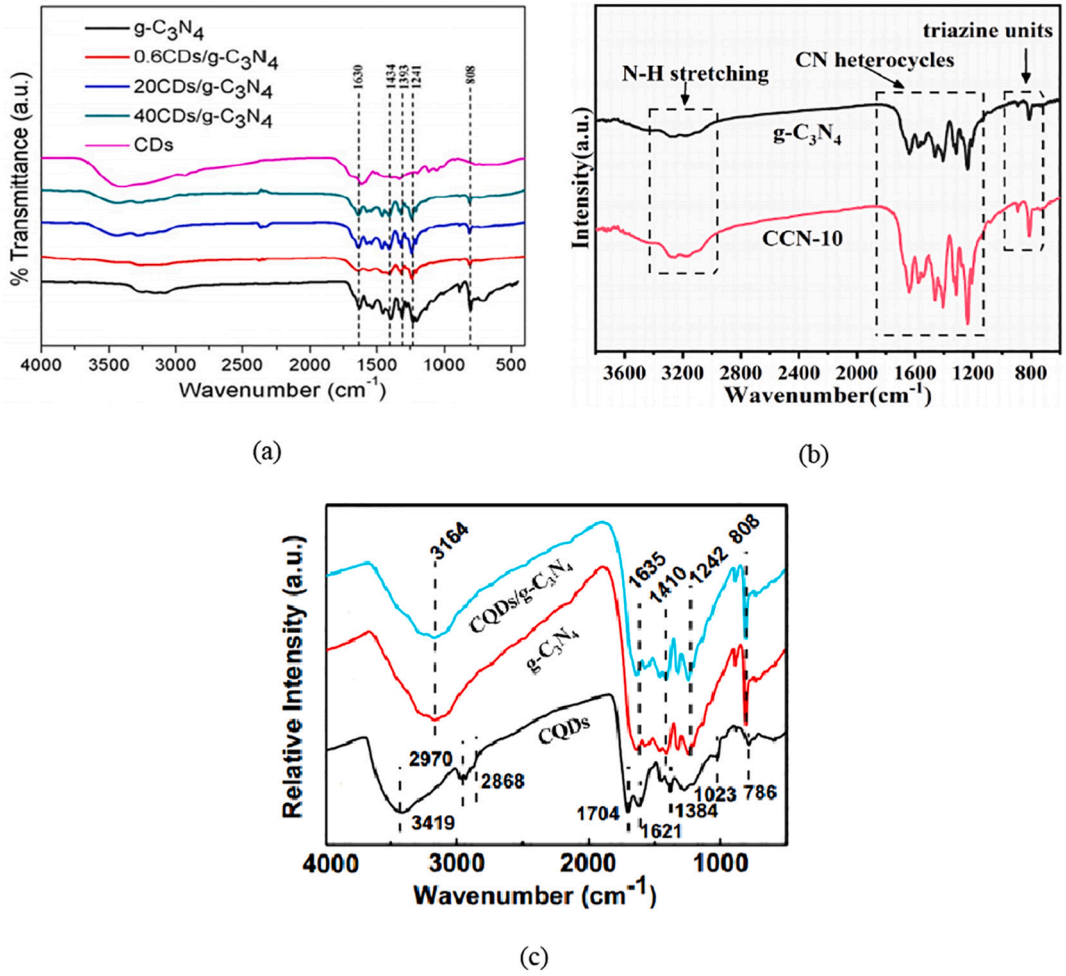


**Fig. 12.** FTIR spectra of (a) CQDs, g-$C_3N_4$, CQD/g-$C_3N_4$ composites [65]; (b) g-$C_3N_4$ and CQD/g-$C_3N_4$ composite [85]; (c) CQDs, g-$C_3N_4$ and CQDs/ g-$C_3N_4$ composite [63].

shows in Fig. 13B1 [29]. Additionally, TEM image of g-$C_3N_4$ revealed a two-dimensional laminated structure [102] in Fig. 13B2 and a flat surface with a sheet-like two dimensional structure [30] as shown in Fig. 13B3. Moreover, a lamellar morphology structure of g-$C_3N_4$ is found according TEM image in Fig. 13B4 [63]. In the TEM image of g-$C_3N_4$ (Fig. 13B5), ripples and wrinkles resembling chiffon were also observed in a two-dimensional layered structure [6].

The successful and uniform distribution of CQDs on the surface of g-$C_3N_4$ is well-defined by the TEM image as displays in Fig. 13C1 to C7. Yet, it is observed from Fig. 13C1 that the surface of acid synthesized CQDs modified g-$C_3N_4$ looks bumpy that indicating a significant loading of foreign substance onto the composite [29]. However, the little shady spots in Fig. 13C2 are expressed the homogenous distribution of biomass synthesized CQDs on the surface of g-$C_3N_4$ [65]. It was also discovered in Fig. 13C3 that CQDs had loaded on the surface of g-$C_3N_4$ and their size harmonised that of pure CQDs [102]. The CQDs/g-$C_3N_4$ samples in Fig. 13C4 similarly exhibit the two-dimensional sheet-like structures, with the exception of a few black dots that are visible on their surfaces [30]. On the other hand, acid synthesized CQDs are uniformly inserted in the porous tubular g-$C_3N_4$ and are identified by a white circle in Fig. 13C5 [100]. Li and coworkers [85] observed that urea synthesized g-$C_3N_4$ is equally dispersed with citric acid synthesized CQDs with an average size of 8 to 10 nm. However, Zhang et al. [6] also applied the same precursors to fabricate CQDs/g-$C_3N_4$ nanocomposite but the composite is not uniformly distributed even though the size of CQDs was 2 to 5 nm (Fig. 13C7). So, synthesize method, temperature, duration and chemicals has the potentiality to enhance the distribution and size of CQDs.

According to the HRTEM image of CQDs/g-$C_3N_4$ (Fig. 13D1), black specks with widths of 2 to 5 nm were seen dispersing uniformly on the surface of g-$C_3N_4$, though some of them consolidated into bigger particles after thermal polymerization [29]. The HRTEM image of CQDs/g-$C_3N_4$ further demonstrated the presence of the usual lattice stripes of 2.09 Å matching to the CQDs (101) facet, supporting the implantation of CQDs onto the g-$C_3N_4$ surface. HRTEM image of CQDs/g-$C_3N_4$ (Fig. 13D2) further confirms the presence of nano sized (1.2 to 4.9 nm) CQDs with lattice fringes of 0.213 nm, which correspond to (100) in-plane lattice spacing of graphene [23,65,93]. It has been discovered in Fig. 13D3 that few black dots are exist in CQDs/g-$C_3N_4$ composite with a size of around 5 nm, and that clearly discernible lattice spacing of 0.321 nm corresponds to the (002) crystal plane of CQDs [30]. Similar lattice spacing (0.326) and crystal plane (002) was observed in Fig. 13D4 but the size of CQDs are in between 2.5 and 3.5 nm that's why CQDs/g-$C_3N_4$ composite is observed as uniformly distributed [46,101]. The interplanar spacing of the CQDs crystallite in the HRTEM pictures (Fig. 13D5—D6) are 0.24 and 0.22 nm, which is equal to the (101) spacing of g-$C_3N_4$ demonstrating their close proximity to one another which favours charge transfer at the interface [23,85,100]. Hydrothermally treated L-Ascorbic acid and melamine synthesized CQDs/g-$C_3N_4$ composite shows a uniform distribution of CQDs (5 nm) on the lamellar surface of the g-$C_3N_4$ [63]. The CQDs are virtually amorphous and have weak crystallization [6], as shown by the HRTEM image that follows in Fig. 13D7. Finally, it can be summarized that there is a major influence of the size of CQDs for the proper distribution on the surface of g-$C_3N_4$ to

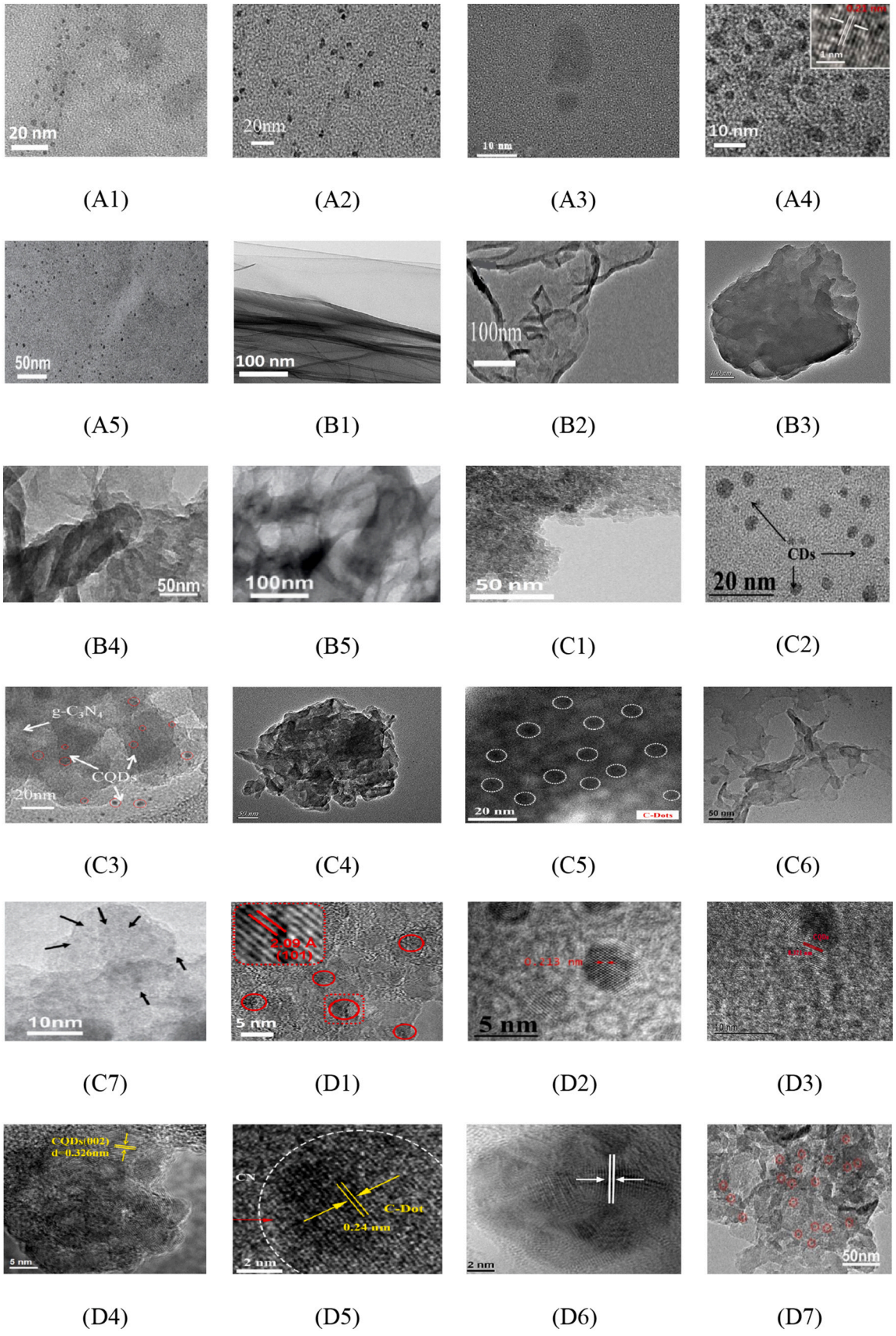


**Fig. 13.** TEM images of CQDs (A1) [29], (A2) [102], (A3) [66], (A4) [31], (A5) [6]; g-$C_3N_4$ (B1) [29], (B2) [102], (B3) [30], (B4) [63], (B5) [6]; CQDs/g-$C_3N_4$ (C1) [29], (C2) [65], (C3) [102], (C4) [30], (C5) [100], (C6) [85], (C7) [6] and HR-TEM image of CQDs/g-$C_3N_4$ (D1) [29], (D2) [65], (D3) [30], (D4) [46], (D5) [100], (D6) [85], (D7) [63].

prepare the ideal CQDs/g-$C_3N_4$ composite. Nevertheless, the discussion shows that CQDs were successfully settled on the surface of g-$C_3N_4$.

#### 4.1.3. X-ray photoelectron spectroscopy (XPS)

Elemental composition and chemical states of CQDs/g-$C_3N_4$ nanocomposite is identified by XPS. Based on elemental percentage in Fig. 14a, CQDs/g-$C_3N_4$ composite has a greater C and N atom ratio than g-$C_3N_4$ [85], which is probably because of the presence of CQDs. Liu and peers [23] also found C, N and O on the surface of CQDs/g-$C_3N_4$ nanocomposite (Fig. 14b). The fundamental heterocycle edifice of g-$C_3N_4$ has been verified by the C1 s and N1 s XPS spectra [101]. According to Zhang et al. [6], CQDs/g-$C_3N_4$ nanocomposite is mostly formed by carbon, nitrogen, and oxygen with photoelectron peaks at 288 (C 1s), 401 (N 1s), and 530 eV (O 1s) (Fig. 14c). CQDs/g-$C_3N_4$ photocatalyst is free of other unintended contaminants and there is only CQDs and g-$C_3N_4$ states is present. Similar photoelectron peaks were observed by Hak and coworkers [65] in their article about biomass synthesis CQDs/g-$C_3N_4$ photocatalyst preparation. The C1s peak was divided into three peaks at energies of 284.77 eV, 287.97 eV, and 288.83 eV, which were assigned to graphitic carbon (C—C), carbonyl (C=O), and $sp^2$ carbon (N-C=N), respectively (Fig. 14d). The major peak at 398.51 eV was attributed to CN=C coordination while the other two faint peaks were attributed to tertiary (N-(C)3) and amino functional groups (C-N-H) at binding energies of 399.80 eV and 400.77 eV, respectively (Fig. 14e). The absorbed water was credited with producing O 1s signal at 531.91 eV (Fig. 14f) that revealing of C—O and C=O bond groups [96].

Besides, due to photoluminescent (PL) effect, CQDs not only act as a photosensitizer and an electron acceptor or mediator to control the flow of charge carriers, but they also act as a semiconducting material to produce photogenerated electron-hole pairs as displays in Fig. 15. The rapid production of charge carriers once sufficient photons has been absorbed over photocatalysts is one of the key concepts in photocatalysis that has the potentiality to enhance the photocatalytic ability of any photocatalysts. However, CQDs has the potentiality to impede the recombination of $e^-/h^+$ pairs, generate charge carriers by converting light with longer wavelengths to light with shorter wavelengths and offers the properties for ideal electron donor/acceptor that finally contributes to potential photocatalytic activity [6,59,80]. In detail, CQDs has the potentiality to enhance the photocatalysis system when it loaded on the surface of g-$C_3N_4$. Due to the photoluminescent effect, CQDs serve as electron receivers or mediators to control the flow of charge carriers, photosensitizers, and electron-hole pairs produced by photosensitizers [6,13,17,65]. Additionally, morphology transformation, heteroatom doping, fabrication of interface heterostructure techniques have the potential to change the electrical structure and surface characteristics of g-$C_3N_4$/CQDs, improving its photocatalytic performance [14,23,103]. The photocatalytic performance of the g-$C_3N_4$/CQDs based heterostructure has been enhanced by the use of CQDs to delay the rate of electron-hole pair recombination. As a result, CQDs are functionalized as spectral convertors due to of exceptional multi-photon illumination property. The wavelength of PL emission is always smaller than the wavelength of practical excitation, according to the up-conversion PL properties [13,88]. The efficiency of CQDs as photocatalysts may also be improved by producing photons with a narrow wavelength by exciting charge carriers at higher wavelengths.

### 4.2. CQDs/g-$C_3N_4$ photocatalyst in dye removal

Photodegradation of dye in wastewater is a research emphasis globally with the aim of preserving the environment and understanding the sustainable advancements of human life. In this context, a metal free and novel g-$C_3N_4$/CQDs photocatalyst is offer a potential prospect to eliminate the dye from wastewater. For example, Zhang and coworkers [6] synthesized g-$C_3N_4$/CQDs photocatalyst by urea and citric acid through an environmentally friendly technique and applied to

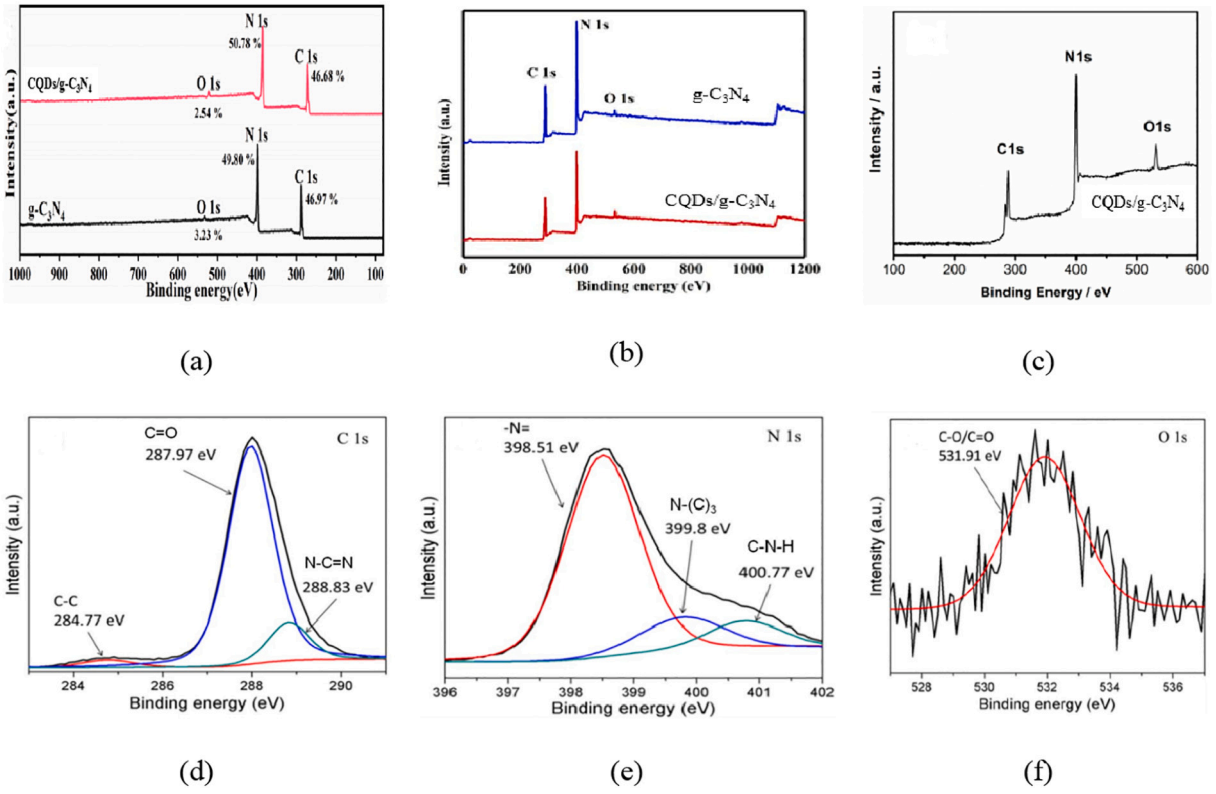


**Fig. 14.** XPS survey spectra of g-$C_3N_4$ and CQDs/g-$C_3N_4$ (a) [85], (b) [23], (c) [6]; (d) C1s of CQDs/g-$C_3N_4$, (e) N1s of CQDs/g-$C_3N_4$ and (f) O1s 0f CQDs/g-$C_3N_4$ [65].

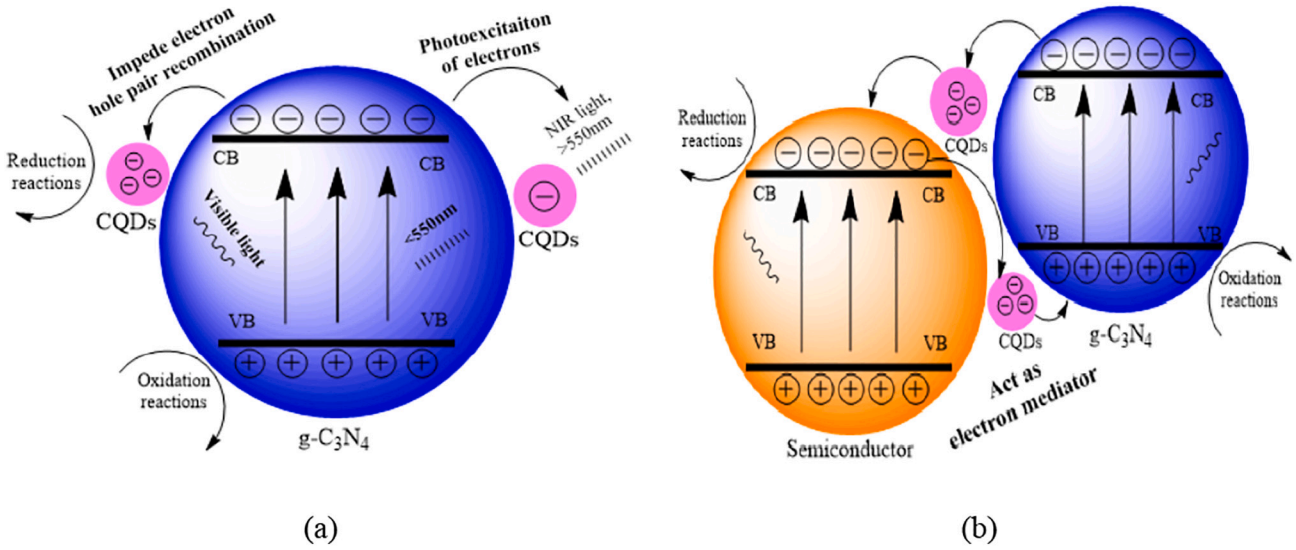


**Fig. 15.** Function of CQDs in pure g-$C_3N_4$ (a) and g-$C_3N_4$/CQDs photocatalyst (b) with improved photocatalytic performance.

degradation of synthetic dye. However, the latent mechanism of charge transfer by g-$C_3N_4$/CQDs nanocomposite for the improvement of photocatalytic performance in terms of dye removal is displays in Fig. 16a. The surface of CQDs/g-$C_3N_4$ is stimulated to produce photogenerated electrons and holes due to the effects of the inner electric arena. The photogenerated holes persisted on the g-$C_3N_4$ whereas the photogenerated electrons quickly moved to the CQDs and producing a spatial separation. The dye molecule was then effectively decomposed through oxidation using the $h^+$ and converted to water, oxygen and others. In addition, while the $O_2$ radicals partially oxidized $H_2O$ to create •OH active species, other radicals also reacted with the organic dye material adsorbed on the surface of g-$C_3N_4$. Since, the positive characteristics of CQDs/g-$C_3N_4$ in VB is higher than the energy level of water ($H_2O$) that's why photo-generated holes are unable to react with $H_2O$ to convert the •OH radicals. Finally, existing holes are engulfed by the oxidation of dye molecules.

Likewise, Gong and peers [80] conducted the fabrication of CQDs/g-$C_3N_4$ by using urea and citrus peel and successfully degreed the sunset yellow dye. They showed the pure individual g-$C_3N_4$ is unable to offer potential photocatalytic efficiency due to large energy gap and the quick recombination of carriers produced by photosynthesis. But interestingly, CQDs induced CQDs/g-$C_3N_4$ composite showed the excellent potentiality in photocatalytic dye degradation under visible light by narrowing the bandgap. According to their findings, $O_2^{\bullet -}$ was the most significant active radical for the photodegradation of sunset yellow dye, followed by $O_2$ and •OH [30,102]. The $E_{VB}$ value of CQDs/g-$C_3N_4$ is lower than the conventional oxidation potential of OH/•OH and $H_2O$/•OH, which prevented the $h^+$ on the VB from directly oxidizing OH or $H_2O$ to generate •OH (Fig. 16b). In order to generate reactive species for CQDs/g-$C_3N_4$ composite during the photocatalytic removal of sunset yellow dye, the suggested reactions are as follows Eqs. (5) to (12).

$$g - C_3N_4 + hv \rightarrow g - C_3N_4\ (e^- + h^+) \quad (5)$$

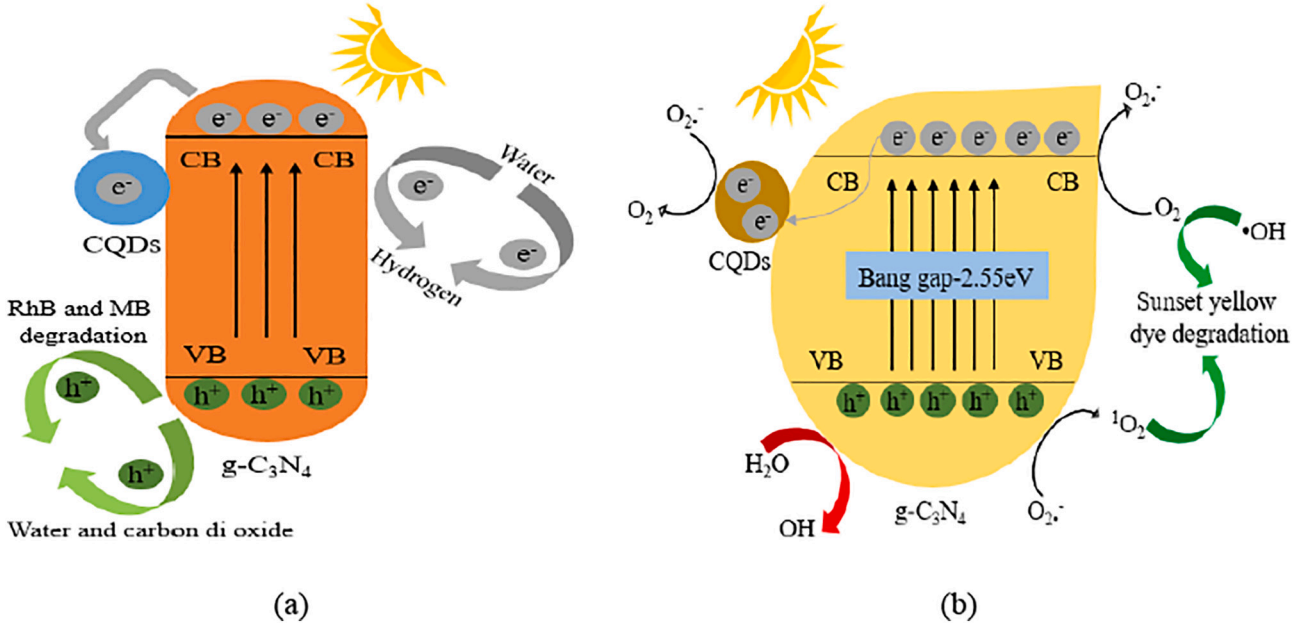


**Fig. 16.** Mechanism of successful dye (a) MB and RhB [6], (b) sunset yellow [80] degradation by using CQDs/g-$C_3N_4$ composite. (For interpretation of the references to colour in this figure legend, the reader is referred to the web version of this article.)

$$g-C_3N_4\ (e^-)+CQDs \rightarrow g-C_3N_4+CQDs\ (e^-) \quad (6)$$

$$g-C_3N_4\ (e^-)+O_2 \rightarrow g-C_3N_4+O_2\cdot^- \quad (7)$$

$$CQDs\ (e^-)+O_2 \rightarrow CQDs+O_2\cdot^- \quad (8)$$

$$O_2\cdot^- + h^+ \rightarrow {}^1O_2 \quad (9)$$

$$O_2\cdot^- + H_2O \rightarrow \cdot OOH + OH^- \quad (10)$$

$$\cdot OOH + H_2O + e^- \rightarrow \cdot OH + OH^- \quad (11)$$

$$\text{Sunset yellow} + \left(O_2\cdot^-/{}^1O_2/\cdot OH\right) \rightarrow \text{Degradation products} \quad (12)$$

Since, there are two processes for the inauguration and conversion of electrons and holes. Firstly, g-$C_3N_4$ is stimulated to produce photogenerated electron-hole pairs in the presence of visible light. In order that the electrons are moving towards the CQDs and form $\bullet O_2^-$ radical by absorbing oxygen. Contaminants are then converted into tiny molecules by the potent oxidative activity of the $\bullet O_2^-$ radical. Additionally, contaminants can be directly oxidized by photogenerated $h^+$ that remains in the VB of g-$C_3N_4$. Secondly, the up-converted PL behaviour of the CQDs allows them to absorb light (>600 nm) and then transmute to shorter wavelengths (<460 nm). The photocatalytic activity can be further increased at shorter wavelengths by excitation of the g-$C_3N_4$ by forming electron-hole pairs [30]. In short, CQDs can boost their ability to capture visible light, which leads to an efficient breakdown of pollutants when exposed to visible light, in addition to improving the photogenerated electron-hole pair's separation. Finally, the above discussion demonstrated that CQDs/g-$C_3N_4$ composite is highly potential than individual CQDs and g-$C_3N_4$ in photocatalytic dye

**Table 2**
Summary of recent published articles supported dye elimination by CQDs/g-$C_3N_4$ photocatalyst.

| Precursors | Synthesis method | Dye | Light Source | Duration | Removal rate | Reference |
|---|---|---|---|---|---|---|
| Citric acid + Urea | Hydrothermal approach | MB<br>RhB | 300 W Xe lamp | 20 min<br>110 min | 100 % | [6] |
| Water hyacinth + Urea | Hydrothermal carbonization | DCPL | Direct sunlight | 120 min | 94.0 % | [65] |
| Glucose + Melamine | Thermal polymerization | MB<br>RhB | NIR light irradiation | 120 min<br>120 min | 86 %<br>38 % | [48] |
| Ethylenediamine-tetraacetic acid + Dicyandiamide | Two-step hydrothermal method | MO | 300 W Xe lamp | 240 min | 91.1 % | [102] |
| Citric acid + Melamine | Low temperate hydrothermal | RhB | Visible light irradiation | 210 min | 95.2 % | [30] |
| Thiourea + Lemon juice | Induction method | RhB | Visible light | 120 min | 90.9 % | [46] |
| Melamine + Cyanuric acid | Calcination method | MB | 300 W Xe lamp | 240 min | 100 % | [100] |
| Citric acid + Urea | Impregnation method | RhB | 500 W Xe lamp | 120 min | 100 % | [23] |
| Citric acid + Melamine | One-pot hydrothermal treatment | Bisphenol A | Near-visible LED | 300 min | 90.4 % | [64] |
| Melamine + $HNO_3/H_2SO_4$ | Spot heating | Bisphenol A | 450 to 850 nm | 120 min | 80 % | [104] |
| Urea + Arabian dates | Hydrothermal carbonization | DCPL | Sunlight irradiation | 90 min | 100 % | [105] |
| Citric acid + Urea | Simple calcination | RhB | 250 W Xe lamp | 20 min | 33 % | [94] |
| Citric acid + Urea | Simple calcination | RhB | 250 W Xe lamp | 40 min | 68 % | [106] |
| Citric acid + Cyanuric acid + Melamine | Solvothermal method | MO | 300 W Xe lamp | 100 min | 93.6 % | [107] |
| Melamine + Citric acid | Hydrothermal | RhB | 300 W Xe lamp | 100 min | 98 % | [108] |
| Citric acid + Urea | Hydrothermal treatment | MB | LED light irradiation | 180 min | 54.60 % | [44] |
| Phenylenediamine + Melamine | Hydrothermal approach | MB | Visible light irradiation | 120 min | 97.9 % | [42] |
| Glucose + Melamine | Simple deposition | RhB | 300 W Xe lamp | 210 min | 100 % | [109] |
| Orange peel + Melamine | Simple impregnation method | MB<br>RhB | 40 W LED bulb | 75 min | 98 %<br>90 % | [110] |
| Melamine + Citric acid | Facile decoration | RhB | 50 W LED lamp | 270 min | 100 % | [111] |
| Melamine + Citric acid + Urea | In-situ calcination and hydrothermal | RhB | 800 W Xe lamp | 45 min | 95 % | [112] |
| Citrus peel + urea | Hydrothermal method | Sunset yellow | 300 W Xenon lamp | 60 min | 96.3 % | [80] |
| Glucose + melamine | Alkali-assisted ultrasonic | Dioxane | LED lamp | 360 min | 77.9 % | [93] |
| Citric acid + Urea | hydrothermal approach | MB | LED light irradiation | 180 min | 54.60 % | [44] |
| Dicyandiamide + Soot of alcohol burner | Calcination | RhB | 3 W LED lamp | k = 0.013 mol L− 1 min − 1 | | [113] |
| Dimethyl sulfoxide + Melamine + Thiourea | One-pot in situ solution polymerization | MO<br>300 W Xe lamp | Visible light | 80 min<br>40 min | 94.3 %<br>100 % | [114] |
| Melamine + Glucose | Simple pyrolysis | RhB | 300 W Xe lamp | 30 min | 97 % | [115] |
| Citric acid + Melamine | Ultrasonic treatment and calcination | RhB | 350 W LED | 30 min | 85 % | [116] |
| Urea + Graphite rods | Hydrothermal method | RhB | 300 W xenon lamp | 90 min | 99.6 % | [117] |
| Graphite rods + Melamine | Simple ultrasonic dispersion | MB | 500 W Xe lamp | 180 min | 97.21 % | [118] |
| Ethylenediamine + Citric acid | Solvothermal | MB<br>RhB<br>MO | 310 W lamp | 60 min | 71 %<br>53.8 %<br>36 % | [119] |
| Citric acid + Melamine | Calcination and microwave oriented self-method | RhB | LED lamp (50 W) | 60 min | 100 % | [120] |
| Melamine + Cyanuric acid + Citric acid | One-step thermal condensation | RhB | 40 W LED lamp | 2.04 $h^{-1}$ 10 $mg^{-1}$ | | [121] |
| Citric acid + Melamine | Facile one-pot co-sintering method | RhB | Nature sunlight | 60 min | 86.1 % ~ 97.2 % | [122] |
| Graphite rods + Urea | Electrostatic adsorption technique | MB | Visible light irradiation | 90 min | >95 % | [123] |
| Pyrene+ Trinitro pyrene + $HNO_3$+ Cyanamide | Electrostatic interactions method | RhB | 300 W Xe lamp | 120 min | 97 % | [124] |

wastewater treatment whereas some examples are given in Table 2.

### 4.3. CQDs/g-$C_3N_4$ photocatalyst in hydrogen evolution

A promising alternative energy source for the future without depending on fossil fuel is the production of hydrogen from water by applying photocatalyst in the presence of solar energy. Hydrogen can be produced in two different ways: photocatalytic water splitting and photocatalytic organic improvement. In order to produce hydrogen, the photocatalytic process typically needs a photocatalyst, reactant, light energy, and photoreactor. Water can occasionally be used as a solitary reactant or in combination with sacrificial agents. Light is required for this, whether visible or UV light, but visible light ensured the absorption range for photocatalysts [23]. It would be necessary for catalyst, reactant, and light to work together effectively for proficient hydrogen generation.

Over the past few years, a significant number of g-$C_3N_4$/CQDs based photocatalysts with improved water splitting performance have been developed [6,101,104]. Under light illumination, the g-$C_3N_4$/CQDs photocatalyst is used for photocatalytic water splitting to produce oxygen and hydrogen. Since, the adsorbed $H_2O$ molecules can become gaseous oxygen and hydrogen when the $e^-/h^+$ pairs move to the surface reaction sites on the g-$C_3N_4$ or CQDs without recombination. In order to separate the filled VB from the empty CB, or vice versa, a semiconductor-based photocatalyst must be illuminated with light that has energy greater than or equal to the band energy of the catalyst. This separation creates the conditions for an electron from the filled valence band to enter the CB legally, which results in the splitting of the $h^+/e^-$ pair. While electrons are used in the reduction process, photogenerated holes are used in the oxidation process [13,48]. Fig. 17a describes the significant phases of photocatalysis and Fig. 17b outlines the stepwise mechanism of photo electrocatalytic water splitting for hydrogen evolution. The symmetry between the catalyst and the carrier species is shown in Eqs. (13) and (14). Eqs. (15) and (16) represents the conversion of water ($H_2O$) into protons ($H^+$) and hydrogen evolution, respectively. The primary duty of the photocatalysis system is to prevent photocatalytic recombination of charge carriers ($e^-/h^+$) in the water splitting process. As seen in Eq. (14), an ineffective heat loss occurs on a mixture of charge carriers. As a result, it is less profitable to produce hydrogen in an aqueous environment.

$$\text{Catalyst} \rightarrow \text{Catalyst}\ (h^+ + e^-) \quad (13)$$

$$\text{Catalyst}\ (h^+ + e^-) \rightarrow \text{Catalyst} \quad (14)$$

$$H_2O + h^+ \rightarrow 1/2\ O_2 + 2H^+ \quad (15)$$

$$2e^- + 2H^+ \rightarrow H_2 \quad (16)$$

Photocatalytic hydrogen evolution mechanism via CQDs/g-$C_3N_4$ photocatalyst is offered and elucidated by Li and peers [85] as shows in Fig. 18a. The bandgap of CQDs/g-$C_3N_4$ photocatalyst in between VB and CB is condensed when CB is easily activated by the electrons in CQDs donor alignment in the presence of visible light. If visible light captured extensively during the hydrogen evolution reaction, then the photogenerated charges are increasing. However, the recombination of photogenerated charges is successfully reduced by the micro-regional heterostructures of CQDs and g-$C_3N_4$, which also encourage the transfer of photogenerated charges across tri-*s*-triazine area. As a result, additional photogenerated electrons transfer to the catalyst and the supporting platinum's surface to take part in the reaction that produces hydrogen. On the other hand, as a sacrifice reagent, triethanolamine (TEOA) can devour holes in the valence band and improve the separation of photogenerated carriers. Consequently, the $H_2$ evolution rates are noticeably improved by all levels of CQDs/g-$C_3N_4$ photocatalyst as shows in Fig. 18a1. Their result shows that CQDs/g-$C_3N_4$ 10 wt% has a $H_2$ evolution rate of 2321 μmol/g/h, which is 7.4 times advanced than pure g-$C_3N_4$. Simultaneously, Wang et al. [63] also found that CQDs/g-$C_3N_4$ 10 wt% photocatalyst offers higher hydrogen evolution rate of 2.2 μmol/h which is approximately 4.4 times that of pure g-$C_3N_4$ (Fig. 18b1). According to the hydrogen evolution mechanism, electron transmission

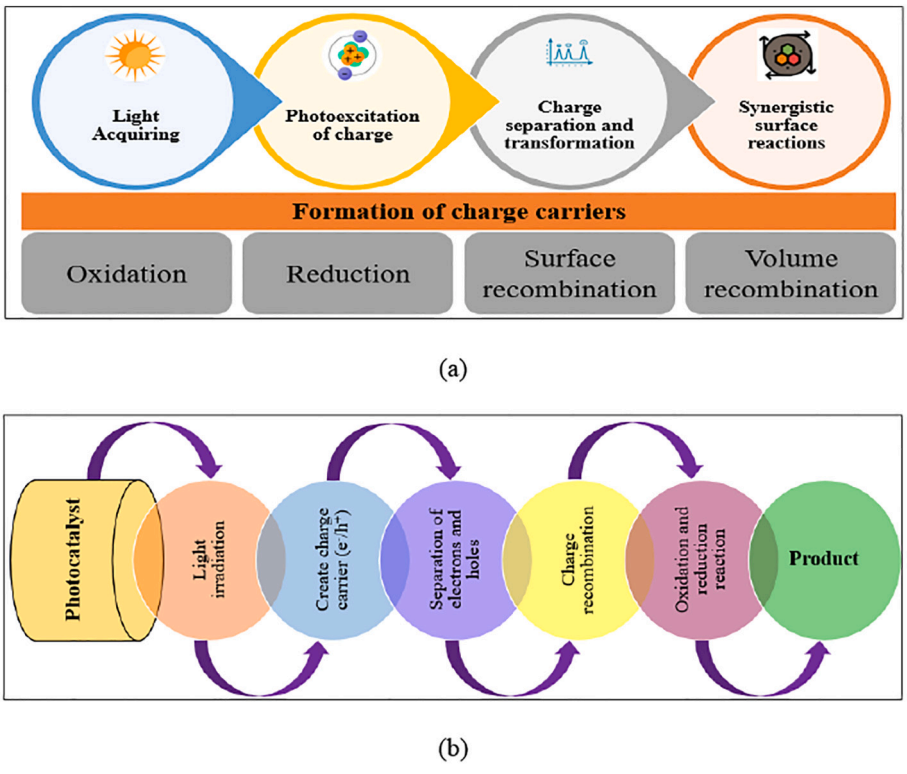


**Fig. 17.** Phases of (a) photocatalysis process and (b) photo electrocatalytic water splitting mechanism for hydrogen evolution.

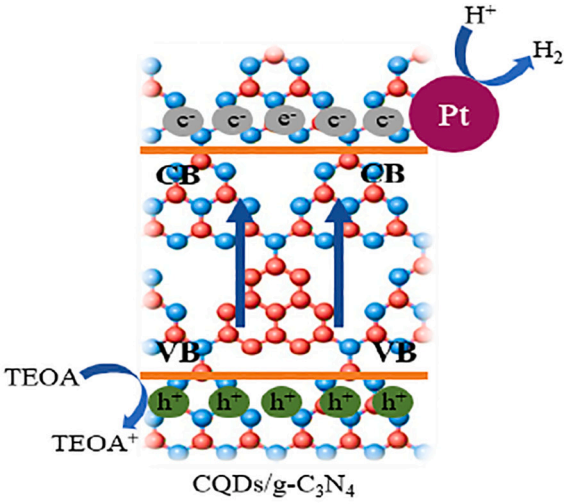


(a)

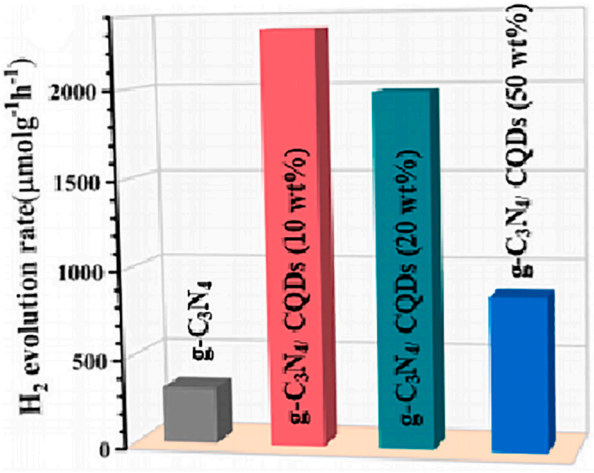


(a1)

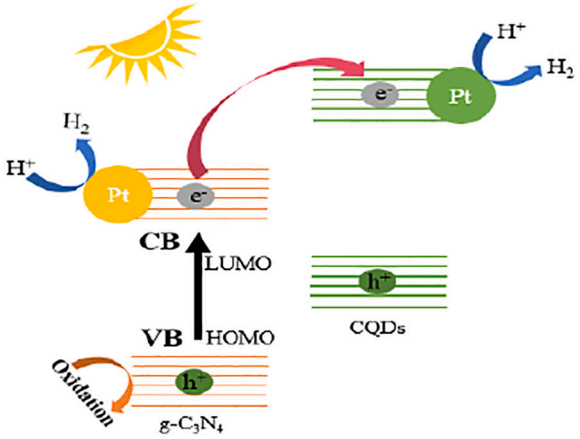


(b)

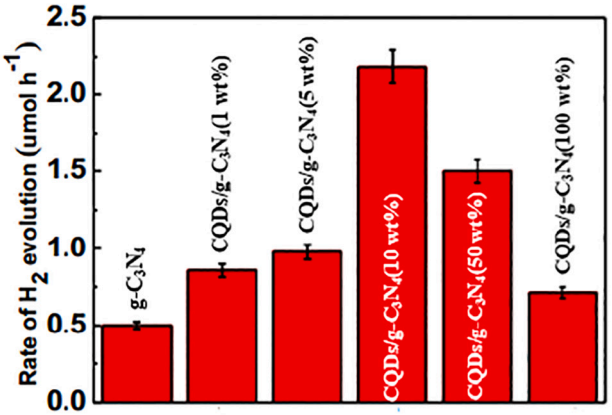


(b1)

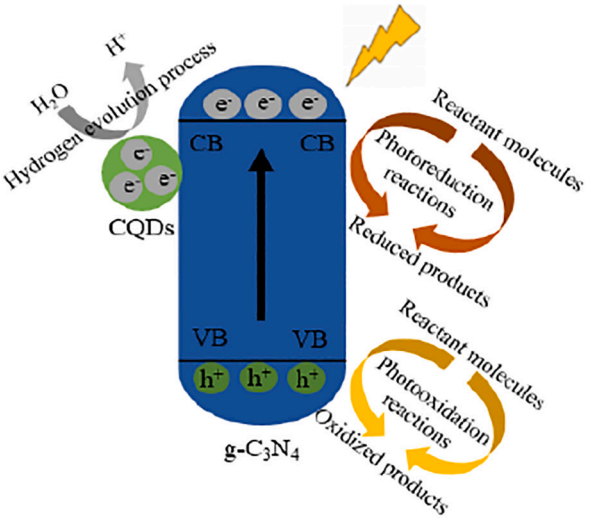


(c)

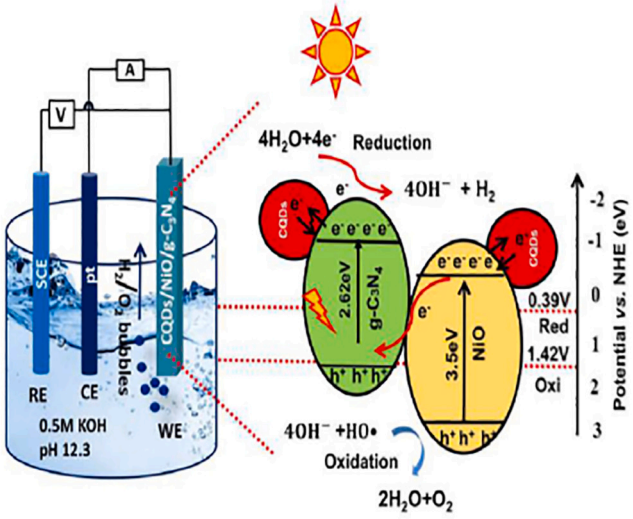


(d)

**Fig. 18.** Photocatalytic hydrogen evolution mechanism and performance through CQDs/g-$C_3N_4$ photocatalyst (a) and (a1) [85]; (b) and (b1) [63]; (c) [6], (d) photo electrochemical water splitting on CQDs modified NiO/g-$C_3N_4$ photo electrode [40].

from the lowest unoccupied molecular orbital (LUMO) of g-$C_3N_4$ towards the LUMO of CQDs is associated with the performance of CQDs/g-$C_3N_4$ photocatalyst. The presence of Pt cocatalyst with CQDs/g-$C_3N_4$ shows the potentiality to enhance photogenerated electrons by its outstanding energetic spots and photocatalytic attribute, as a result $H_2O$ easily diverted to hydrogen (Fig. 18b). However, a research by Zhang and team [6] applied urea and citric acid as a precursor to fabricate CQDs/g-$C_3N_4$ photocatalyst similarly potential to produce hydrogen effectively. The maximum hydrogen evolution rate was 664 μmol/h/g that is offered by CQDs/g-$C_3N_4$ 0.98 wt% photocatalyst. The photocatalytic hydrogen evolution mechanism demonstrates that the photogenerated electrons of g-$C_3N_4$ simply moved towards CQDs due to the effect of internally charged. Since, the photogenerated holes persisted on the g-$C_3N_4$ and creates a spatial gap. Subsequently, the photogenerated holes are then occupied by $H^+$ to produce hydrogen (Fig. 18c).

According to Noor et al. [40] urea, thiourea and citric acid induced CQDs/NiO/g-$C_3N_4$ photocatalyst offers outstanding performance in hydrogen evolution as well as dye removal and oxygen evolution. In the application they applied photo electrochemical water splitting that shows a reduction of band-gap values from 2.62 to 1.8 eV in UV Visible spectra of nanocomposites confirmed an improvement towards red shift. Where electrochemical impedance spectroscopy (EIS) performance was evaluated in 0.5 M KOH electrolyte maintain at neutral pH ~12.3 under $\lambda > 420$ nm irradiation. On the exposure of incident light on the photoanode, electrons from VB migrate to CB of NiO/g-$C_3N_4$ generate the photoelectrons which further move to from CB of NiO to VB of g-$C_3N_4$ and to surface of CQDs for space charge separation under z-scheme mechanism as explained in Fig. 18d. Similarly Pan and team [125] and Wang and co-researcher [126] applied photocatalytic water splitting for the production of hydrogen by using g-$C_3N_4$/$TiO_2$/CQDs composite photocatalyst.

On the other hand, Vogt and team [127] applied Steam and Dry Methane Reforming (S/DMR) process for the production of hydrogen (Steam: $CH_4 + H_2O \rightarrow CO + 3H_2$ and Dry: $CH_4 + CO_2 \rightarrow 2CO + 2H_2$). In addition, Nishimura and his research group [128] investigated the effect of pressure of sweep gas on a biogas dry reforming to get $H_2$. The highest concentration of $H_2$ is obtained in the case of the molar ratio of $CH_4$:$CO_2$ = 1:1. However, several challenges such as catalyst deactivation and the low $H_2$/CO ratio of the syngas produced are limits the performance of hydrogen evolution by applying DMR method [129]. Table 3 shows an overview of recent studies on the performance of photocatalytic hydrogen evolution by applying CQDs/g-$C_3N_4$ photocatalyst. In summary, the synthesized CQDs/g-$C_3N_4$ photocatalyst had an advanced photocatalytic efficiency for photocatalytic dye wastewater treatment and energy recovery by generating hydrogen.

## 5. SWOT analysis

The Strengths, Weaknesses, Opportunities, and Threats (SWOT) analysis for the use of CQDs/g-$C_3N_4$ photocatalyst in dye removal and hydrogen production has been carried out by considering social, economic and environmental sustainability perceptions as shown in the Fig. 19.

### 5.1. Strengths (S)

Mostly, carbon and nitrogen induced raw materials are applied for the synthesis of CQDs/g-$C_3N_4$ photocatalyst, which acts as a feasible, green and sustainable precursors [6,121,138]. Numerous studies have looked at the quick and efficient synthesis of CQDs/g-$C_3N_4$ using cutting-edge techniques during the last few decades. Additionally, the procedure produces a good yield, emits fewer emissions, and doesn't need any harmful solvents. It is also industry-friendly due to its simple synthesis and fast production, which opens up new possibilities for its use in a variety of applications, for example water treatment, gas capturing, pollutants degradation, biosensing, biomedical, bioimaging, $CO_2$ mitigation process and hydrogen production [6,44,46,111,138]. During the function of CQDs/g-$C_3N_4$ photocatalyst in dye removal and hydrogen evolution, electron donor-acceptor properties of CQDs is

**Table 3**
Summary of recent published articles supported hydrogen evolution by CQDs/g-$C_3N_4$ photocatalyst.

| Precursor | Synthesis Method | Light Source | $H_2$ Evolution Rate | Reference |
|---|---|---|---|---|
| Citric acid + Urea | Hydrothermal approach | 300 W Xe lamp | 1291 μmol/g/h | [6] |
| Melamine + Cyanuric acid | Calcination method | 300 W Xe lamp | 24,760 μmol/g/h | [100] |
| Citric acid + Urea | Hydrothermal method | 300 W Xe lamp | 2321 μmol/g/h | [85] |
| Citric acid + Urea | Impregnation method | 300 W Xe lamp | 626.93 μmol/h/g | [23] |
| Citric acid + Urea + Melamine | Solvothermal method | Visible light irradiation | 987.4 μmol/g/h | [31] |
| L-ascorbic acid + Melamine | Hydrothermal approach | UV light irradiation | 2.2 μmol/h | [63] |
| Urea + Chitosan + Acetic acid | Hydrothermal treatment | Visible light irradiation | 295.9 μmol/g/h | [101] |
| Urea + Citric acid | Thermal polymerization | 300 W xenon lamp | 3538.3 μmol/g/h | [45] |
| Melamine + $HNO_3$/$H_2SO_4$ | Spot heating | 450–850 nm | 152 μmol/g/h | [104] |
| Urea + Glucose | Thermal polymerization | Visible light | 2.34 mmol/g/h | [130] |
| Citric acid + Melamine | Free-template chemical method | 40 W LED lamp | 382 μmol/g/h | [131] |
| Urea + Glucose | Alkali-auxiliary sonication method | 300 W Xe lamp | 220.77 μmol/g/h | [132] |
| Sucrose + Melamine | Hydrothermal method | 300 W Xe lamp | 4.134 μmol/g/h | [125] |
| Flower bee pollens + Dicyandiamide | Hydrothermal | 300 W Xenon lamp | 88.1 μmol/h | [133] |
| Melamine + L-Ascorbic acid | Hydrothermal | 3 W Four low power LEDs | 183 μmol/h | [63] |
| Citric acid + Urea | Homogeneous thermal pyrolysis | 300 W Xenon lamp | 27.6 μmol/h | [134] |
| Dicyandiamide + Aminohexanoic acid | Solvothermal | 300 W Xe arc lamp | 116.1183 μmol/h | [135] |
| Urea + Graphite rod | Solvothermal and physical co-precipitation methods | Visible-light irradiation | 9.4 μmol/g/h | [136] |
| Candle soot + Urea + Melamine | Impregnation precipitation methods | 350 W Xe arc lamp | 10.9 μmol/h | [137] |
| Melamine + Urea | Hydrothermal treatment | 300 W Xe-lamp | 70.05 10.9 μmol/h | [72] |
| Dicyandiamide | Calcination | 3 W LED lamp | 218 μmol/g/h | [113] |
| Urea + Graphite rods | Hydrothermal method | 300 W xenon lamp | 2.169 μmol/g/h | [117] |
| Dicyandiamide + Citric acid | One-step thermal polymerization | 300 W Xenon arc lamp | 3319.3 μmol/g/h | [41] |
| Citric acid + Urea | Colloidal template crystal method | 250 W xenon lamp | 8.12 mmol/g/h | [138] |
| Urea + Dopamine hydrochloride | Impregnated calcination | 300 W Xe lamp | 712.90 μmol/g/h | [139] |
| Urea + Thiourea + citric acid | Wet chemical method | $\lambda > 420$ nm irradiation | ~ – 19 $mAcm^{-2}$ at potential 0.39 V | [40] |
| Melamine + sucrose + tetrabutyl titanate | Thermal polycondensation | Xenon lamp (300 W) | 6.497 μmol/gh | [125] |
| Citric acid + dicyandiamide | Thermo-polymerization | Xenon arc lamp (300 W) | 2.34 μmol/gh | [126] |


**Fig. 19.** SWOT analysis of using CQDs/g-$C_3N_4$ photocatalyst in energy and environmental applications.

possess outstanding performance under light illumination. CQDs have an enormously lucrative role in the charge transfer and separation process for the growth of CQDs/g-$C_3N_4$ photocatalyst [61]. On the other hands, due to the exhaustion of fossil fuels, water bodies are becoming more and more polluted, rendering them unfit for human consumption and causing an increase in the energy crisis. Therefore, CQDs/g-$C_3N_4$ photocatalyst acts as a sustainable and environmentally beneficial technology that offers decent financial aids with the favourable synthesis of hydrogen energy and fresh water. More importantly, the produced green hydrogen will be ensured the future fuel demands and the fresh water can be reuse in domestic, commercial and irrigation purposes.

### 5.2. Weakness (W)

Unique and advance synthesis method is one of the main drawbacks of CQDs/g-$C_3N_4$ photocatalyst. Appropriate synthesis process has the potentiality to prepare pure and quality products as well as highly efficient and stable photocatalyst [140]. Synthesis process can identify various morphologies, but it is unknown how they relate to one another specifically. Moreover, there is inadequate relationship between catalytic activity and morphology of CQDs/g-$C_3N_4$ photocatalyst. Consequently, the dye removal performance still not hundred percent successful and hydrogen evolution rate also not satisfactory. However, the presence of inappropriate bang gap in the mechanism also enhances the performance of the photocatalyst. There is also an influence of time, catalyst dose, reaction, temperature, pH and light irradiation in the performance of CQDs/g-$C_3N_4$ photocatalyst. Environmental and social impact assessment need to carryout prior to apply in large scale industry level. Additionally, there are currently no restrictions in national and global level that apply to carbon and nitrogen constructed nanomaterials.

### 5.3. Opportunities (O)

CQDs/g-$C_3N_4$ is a promising photocatalyst for several sectors such as energy, environment, medical, harmful gas control, contaminants and heavy metals control [141]. One of the most important advantages of CQDs/g-$C_3N_4$ is workable in visible light irradiation. Which typically reduce the cost and makes the photocatalyst environmentally friendly by using nature-based power. CQDs/g-$C_3N_4$ offers outstanding photostability and recyclability for the degradation of pollutants. CQDs functions as a photosensitizer, causing g-$C_3N_4$ to absorb more visible light as a result of its up-converted photoluminescence feature and inducing g-$C_3N_4$ to form more electron-hole pairs and reactive $^{\bullet}O_2$ and $^{\bullet}OH$ radicals. CQDs serve as electron-sinks in the g-$C_3N_4$ VB, where they can capture photoexcited electrons and keep them from recombining with photogenerated holes [44]. In the near future, it can be further investigated for semiconductor photocatalysis to purify water, nanohybrid light-driven catalyst to remove heavy metal contaminants, and in the animal and human health sectors. Semiconductor photocatalysis is an auspicious technology due to its ability to directly transform solar energy into chemical energy and for being ecologically friendly.

### 5.4. Threats (T)

Although employing CQDs/g-$C_3N_4$ to generate hydrogen is a favourable strategy, it is still in the early stages of development. It's important to fully comprehend the effects of operating variables like pH, temperature, wetness and calcination prior to large scale production. On the other hand, there is a possibility to generate harmful byproducts during the application of CQDs/g-$C_3N_4$ in pollutants removal. Although, the use of strong acid to synthesize CQDs/g-$C_3N_4$ photocatalyst offers an excellent outcome in photocatalytic applications. So, toxicological effects of dye removal and hydrogen evolution process should be examined to ensure human safety and environmental sustainability. In this regard, a life cycle assessment (LCA) tools can be applied for suitability checking of a system or process and to take the proper initiatives about the use of any technology and potential to identify the risks.

## 6. Conclusion and future perspective

Here, this review offers a comprehensive review and detail discussion of green and non-metal g-$C_3N_4$/CQDs photocatalyst for photocatalysis. It also presents an assessment of current developments of CQDs/g-$C_3N_4$ photocatalyst in conjunction with the synthesis procedures, photocatalytic enrich mechanisms, modifications, dopant incorporation and photocatalytic applications in energy and environmental area. It was demonstrated that the optical and electrical features of g-$C_3N_4$ were smartly improved by the incorporation of CQDs, resulting in a notable increase in quantum efficiency for the photocatalytic properties. More importantly, CQDs modified g-$C_3N_4$ not only overcome the shortfalls of g-$C_3N_4$ but also exhibits the potentiality to prevent recombining of charge carriers, encouraged photogenerated $e^-/h^+$ separation and visible light absorption capacity by maintaining photostability which enhanced photocatalytic activity, contribution and overall performance. A stunning manifestation of CQDs/g-$C_3N_4$ in hydrogen evolution and degradation of dye molecules makes the composite an excellent safeguard against environmental degradation and energy crisis. In addition, CQDs/g-$C_3N_4$ composite is widely applied in $CO_2$ reduction, elimination of bacteria, biosensing, organic pollutants degradation, heavy metal detection and removal that also contributes for sustainable environment.

Although, there has undoubtedly been successful and significant achievements of CQDs/g-$C_3N_4$ photocatalyst, but the progress condition is still at initial phases. However, it is confessed that there are many silent challenges that must be overcome in order to better meet the demands of practical application of resolving the energy and environmental issues. As a result, the features that need for more investigation in order to effectively apply CQDs/g-$C_3N_4$ photocatalyst is suggested. Some crucial hushed points are explained as follow.

- In order to synthesize CQDs/g-$C_3N_4$, it is critical to produce simple, efficient, cheap, and environmentally friendly techniques. The suitable CQDs and g-$C_3N_4$ should have low costs, high fluorescence quantum yields, stable, toxic-free, and narrow particle size distributions from nature-based carbon rich biomass source. It is crucial to develop effective techniques for loading CQDs onto g-$C_3N_4$ photocatalysts by choosing appropriate precursors and enhancing their recyclability. In addition, the use of strong acid or base should be prohibited during the synthesis process to avoid environmental and human insecurity.
- The fabrication process of CQDs/g-$C_3N_4$ mostly depends on thermal carbonization in conjunction of high temperature resulting inconsistency and unregulated outcomes that has the potentiality to make barrier in photocatalytic performance. Even though the self-assembled fabricated method of CQDs/g-$C_3N_4$ is reasonably straightforward that possess a sloppy coupling interface that hampers operative charge carriers. The exploration of more sophisticated synthesis methods will be more demandable in current era with focusing distinguished development of photocatalytic ability.
- Laterally, the frequent shaky connection in the interface of CQDs/g-$C_3N_4$ typically prevents the energy level adjustment and fluent charge transfer, means that there is still room for improvement in the synthesis techniques. To maximize the efficiency of the photocatalyst, some forthright green synthesis approaches are desperately needed.
- In order to produce g-$C_3N_4$ with higher surface areas, several morphologies can be investigated, including nanotubes, nanofibers, nanosheets, nanorods, nanospheres structures and so on. Furthermore, it is important to investigate the initial loading volume and size of CQDs and element doping that also can be contribute in the improvements of photocatalytic performance of CQDs/g-$C_3N_4$.
- To date, advance prospect of CQDs/g-$C_3N_4$ is typically enhanced, limited and depends on the unsatisfactory hypothetical and practical exercise. The potentiality of CQDs/g-$C_3N_4$ can be continued in conjunction with modern intelligence materials-oriented chemistry laboratory research discoveries.
- The relationship between charge carrier movement kinetics and structural characteristics of CQDs/g-$C_3N_4$ photocatalysts should be precisely demonstrated and verified in future research. To develop highly effective visible-light induced photocatalysts, organised research is required for the incorporation of various semiconductors and ingredients with CQDs/g-$C_3N_4$.
- It is still challenging and crucial to establish CQDs/g-$C_3N_4$ fabrication methods and machineries for industrial application as CQDs/g-$C_3N_4$ photocatalyst research is currently only at the laboratory level. The development of a multifunctional synergistic platform and the suitable integration of the related photocatalytic application systems will become popular subjects.
- Since, CQDs/g-$C_3N_4$ novel photocatalyst is mostly applied and concentrated in the degradation of contaminants and hydrogen generation. The application of CQDs/g-$C_3N_4$ photocatalyst in biosensing, biomedical, bacterial disinfection, oxygen evolution, food security and energy storage will be popular research arena. Additionally, CQDs/g-$C_3N_4$ photocatalyst can be highly potential for the expansion of solar cell industries.
- Subsequently, it is significantly important to prevent hazardous byproduct and gas ($CO_2$) during the photodegradation of contaminants and energy generation to develop an innovative research theme which will be completely green.

According to the above discussions, it is projected that the affordable, eco-friendly.

CQDs/g-$C_3N_4$ photocatalyst will play a significant role in a variety of photocatalytic processes. It is anticipated that the suggested outline of the development path in CQDs/g-$C_3N_4$ will provide scholars with complete information that will enable them to understand the main ideas and potential for the future developments of any composite photocatalysts. This review is intended to give readers a comprehensive understanding of the application and continuous growth of CQDs/g-$C_3N_4$ in energy and environmental sectors.

## Declaration of competing interest

The authors declare that they have no known competing financial interests or personal relationships that could have appeared to influence the work reported in this paper.

## Data availability

Data will be made available on request.

## Acknowledgements

This study was supported by the Universiti Malaysia Pahang Al-Sultan Abdullah (UMPSA) internal grant, International Publication Grant (RDU 213305). The authors express gratitude for the grant.

## References

[1] X. Liu, R. Ma, L. Zhuang, B. Hu, J. Chen, X. Liu, X. Wang, Recent developments of doped g-C3N4 photocatalysts for the degradation of organic pollutants, Crit. Rev. Environ. Sci. Technol. 51 (2021) 751–790, https://doi.org/10.1080/10643389.2020.1734433.

[2] H.M. Solayman, A. Hossen, A. Abd, N. Yahida, K. Hon, L. Ching, M. Uddin, K. Zoh, Performance evaluation of dye wastewater treatment technologies : a review, J. Environ. Chem. Eng. 11 (2023), 109610, https://doi.org/10.1016/j.jece.2023.109610.

[3] F.S. Mustafa, K.H. Hama Aziz, Heterogeneous catalytic activation of persulfate for the removal of rhodamine B and diclofenac pollutants from water using iron-impregnated biochar derived from the waste of black seed pomace, Process Saf. Environ. Prot. 170 (2023) 436–448, https://doi.org/10.1016/j.psep.2022.12.030.

[4] K.H. Hama Aziz, Application of different advanced oxidation processes for the removal of chloroacetic acids using a planar falling film reactor, Chemosphere 228 (2019) 377–383, https://doi.org/10.1016/j.chemosphere.2019.04.160.
[5] D. Ma, H. Yi, C. Lai, X. Liu, X. Huo, Z. An, L. Li, Y. Fu, B. Li, M. Zhang, L. Qin, S. Liu, L. Yang, Critical review of advanced oxidation processes in organic wastewater treatment, Chemosphere 275 (2021), https://doi.org/10.1016/j.chemosphere.2021.130104.
[6] L. Zhang, J. Zhang, Y. Xia, M. Xun, H. Chen, X. Liu, X. Yin, Metal-free carbon quantum dots implant graphitic carbon nitride: enhanced photocatalytic dye wastewater purification with simultaneous hydrogen production, Int. J. Mol. Sci. 21 (2020), https://doi.org/10.3390/ijms21031052.
[7] A.A. Aziz, C.K. Cheng, S. Ibrahim, M. Matheswaran, P. Saravanan, Visible light improved, photocatalytic activity of magnetically separable titania nanocomposite, Chem. Eng. J. 183 (2012) 349–356, https://doi.org/10.1016/j.cej.2012.01.006.
[8] Y. Xiao, Z. He, R. Wang, X. Tao, B. Li, Synthesis of WO3 nanofibers decorated with BiOCl nanosheets for photocatalytic degradation of organic pollutants under visible light, Colloids Surfaces A Physicochem. Eng. Asp. 580 (2019), 123752, https://doi.org/10.1016/j.colsurfa.2019.123752.
[9] M. Ismael, E. Elhadad, M. Wark, Construction of SnO2/g-C3N4 composite photocatalyst with enhanced interfacial charge separation and high efficiency for hydrogen production and rhodamine B degradation, Colloids Surfaces A Physicochem. Eng. Asp. 638 (2022), 128288, https://doi.org/10.1016/j.colsurfa.2022.128288.
[10] M. Ismael, Enhanced photocatalytic hydrogen production and degradation of organic pollutants from Fe (III) doped TiO2 nanoparticles, J. Environ. Chem. Eng. 8 (2020), 103676, https://doi.org/10.1016/j.jece.2020.103676.
[11] F. Ming, J. Hong, X. Xu, Z. Wang, Dandelion-like ZnS/carbon quantum dots hybrid materials with enhanced photocatalytic activity toward organic pollutants, RSC Adv. 6 (2016) 31551–31558, https://doi.org/10.1039/c6ra02840c.
[12] M. Ismael, The photocatalytic performance of the ZnO/g-C3N4 composite photocatalyst toward degradation of organic pollutants and its inactivity toward hydrogen evolution: the influence of light irradiation and charge transfer, Chem. Phys. Lett. 739 (2020), 136992, https://doi.org/10.1016/j.cplett.2019.136992.
[13] S. Patial, A. Sonu, N. Sudhaik, T. Chandel, P. Ahamad, P. Raizada, N. Singh, R. Selvasembian Chaukura, A review on carbon quantum dots modified g-C3N4-based photocatalysts and potential application in wastewater treatment, Appl. Sci. 12 (2022), https://doi.org/10.3390/app122111286.
[14] Y. Chen, X. Bai, A review on quantum dots modified g-C3N4-based photocatalysts with improved photocatalytic activity, Catalysts 10 (2020), https://doi.org/10.3390/catal10010142.
[15] Z.W. Heng, W.C. Chong, Y.L. Pang, C.H. Koo, An overview of the recent advances of carbon quantum dots/metal oxides in the application of heterogeneous photocatalysis in photodegradation of pollutants towards visible-light and solar energy exploitation, J. Environ. Chem. Eng. 9 (2021), 105199, https://doi.org/10.1016/j.jece.2021.105199.
[16] S. Sekar, S. Lee, P. Vijayarengan, K.M. Kalirajan, T. Santhakumar, S. Sekar, S. Sadhasivam, Upcycling of wastewater via effective photocatalytic hydrogen production using MnO2 nanoparticles—decorated activated carbon nanoflakes, Nanomaterials 10 (2020) 1–12, https://doi.org/10.3390/nano10081610.
[17] C. Tang, C. Liu, Y. Han, Q. Guo, W. Ouyang, H. Feng, M. Wang, F. Xu, Nontoxic carbon quantum dots/g-C3N4 for efficient photocatalytic inactivation of Staphylococcus aureus under visible light, Adv. Healthc. Mater. 8 (2019) 1–8, https://doi.org/10.1002/adhm.201801534.
[18] M. Ismael, One-step ultrasonic-assisted synthesis of Ni-doped g-C3N4 photocatalyst for enhanced photocatalytic hydrogen evolution, Inorg. Chem. Commun. 151 (2023), 110607, https://doi.org/10.1016/j.inoche.2023.110607.
[19] M. Ismael, A review on graphitic carbon nitride (g-C3N4) based nanocomposites: synthesis, categories, and their application in photocatalysis, J. Alloys Compd. 846 (2020), 156446, https://doi.org/10.1016/j.jallcom.2020.156446.
[20] M. Ismael, M. Wark, Photocatalytic activity of CoFe2O4/g-C3N4 nanocomposite toward degradation of different organic pollutants and their inactivity toward hydrogen production: the role of the conduction band position, FlatChem 32 (2022), 100337, https://doi.org/10.1016/j.flatc.2022.100337.
[21] M. Ismael, Facile synthesis of NiO-loaded g-C3N4 heterojunction photocatalyst for efficient photocatalytic degradation of 4-nitrophenol under visible light irradiation, J. Photochem. Photobiol. A Chem. 439 (2023), 114576, https://doi.org/10.1016/j.jphotochem.2023.114576.
[22] M. Ismael, Structure, properties, and characterization of mullite-type materials Bi2M4O9and their applications in photocatalysis: a review, J. Environ. Chem. Eng. 10 (2022), 108640, https://doi.org/10.1016/j.jece.2022.108640.
[23] H. Liu, J. Liang, S. Fu, L. Li, J. Cui, P. Gao, F. Zhao, J. Zhou, N doped carbon quantum dots modified defect-rich g-C3N4 for enhanced photocatalytic combined pollutions degradation and hydrogen evolution, Colloids Surfaces A Physicochem. Eng. Asp. 591 (2020), https://doi.org/10.1016/j.colsurfa.2020.124552.
[24] X. Wang, K. Maeda, A. Thomas, K. Takanabe, G. Xin, J.M. Carlsson, K. Domen, M. Antonietti, A metal-free polymeric photocatalyst for hydrogen production from water under visible light, Nat. Mater. 8 (2009) 76–80, https://doi.org/10.1038/nmat2317.
[25] M. Bellardita, E.I. García-López, G. Marcì, I. Krivtsov, J.R. García, L. Palmisano, Selective photocatalytic oxidation of aromatic alcohols in water by using P-doped g-C3N4, Appl. Catal. Environ. 220 (2018) 222–233, https://doi.org/10.1016/j.apcatb.2017.08.033.
[26] G. Li, Z. Lian, W. Wang, D. Zhang, H. Li, Nanotube-confinement induced size-controllable g-C3N4 quantum dots modified single-crystalline TiO2 nanotube arrays for stable synergetic photoelectrocatalysis, Nano Energy 19 (2016) 446–454, https://doi.org/10.1016/j.nanoen.2015.10.011.
[27] M. Ismael, Y. Wu, D.H. Taffa, P. Bottke, M. Wark, Graphitic carbon nitride synthesized by simple pyrolysis: role of precursor in photocatalytic hydrogen production, New J. Chem. 43 (2019) 6909–6920, https://doi.org/10.1039/c9nj00859d.
[28] M. Ismael, Y. Wu, M. Wark, Photocatalytic activity of ZrO2 composites with graphitic carbon nitride for hydrogen production under visible light, New J. Chem. 43 (2019) 4455–4462, https://doi.org/10.1039/c8nj06507a.
[29] G. Di, Z. Zhu, Q. Dai, H. Zhang, X. Shen, Y. Qiu, Y. Huang, J. Yu, D. Yin, S. Küppers, Wavelength-dependent effects of carbon quantum dots on the photocatalytic activity of g-C3N4 enabled by LEDs, Chem. Eng. J. 379 (2020), 122296, https://doi.org/10.1016/j.cej.2019.122296.
[30] Y. Hong, Y. Meng, G. Zhang, B. Yin, Y. Zhao, W. Shi, C. Li, Facile fabrication of stable metal-free CQDs/g-C3N4 heterojunctions with efficiently enhanced visible-light photocatalytic activity, Sep. Purif. Technol. 171 (2016) 229–237, https://doi.org/10.1016/j.seppur.2016.07.025.
[31] W. Shi, J. Wang, S. Yang, X. Lin, F. Guo, J. Shi, Fabrication of a ternary carbon dots/CoO/g-C3N4 nanocomposite photocatalyst with enhanced visible-light-driven photocatalytic hydrogen production, J. Chem. Technol. Biotechnol. 95 (2020) 2129–2138, https://doi.org/10.1002/jctb.6398.
[32] Z. Jiang, W. Wan, H. Li, S. Yuan, H. Zhao, P.K. Wong, A hierarchical Z-scheme α-Fe2O3g-C3N4 hybrid for enhanced photocatalytic CO2 reduction, Adv. Mater. 1706108 (2018).
[33] X. Yan, H. An, Z. Chen, G. Yang, Significantly enhanced charge transfer efficiency and surface reaction on NiP2/g-C3N4 heterojunction for photocatalytic hydrogen evolution, Chinese J. Chem. Eng. 43 (2022) 31–39, https://doi.org/10.1016/j.cjche.2021.12.019.
[34] Y. Liao, C. Zou, H. Peng, S. Lin, W. Chen, Y. Cao, B. Li, A novel g-C3N4/BiOI/Ag2WO4 heterojunction for efficient degradation of organic pollutants under visible light irradiation, Ceram. Int. 47 (2021) 26248–26259, https://doi.org/10.1016/j.ceramint.2021.06.033.
[35] M.J. Lima, A.M.T. Silva, C.G. Silva, J.L. Faria, Graphitic carbon nitride modified by thermal, chemical and mechanical processes as metal-free photocatalyst for the selective synthesis of benzaldehyde from benzyl alcohol, J. Catal. 353 (2017) 44–53, https://doi.org/10.1016/j.jcat.2017.06.030.
[36] C. Prasad, H. Tang, Q. Liu, I. Bahadur, S. Karlapudi, Y. Jiang, A latest overview on photocatalytic application of g-C3N4 based nanostructured materials for hydrogen production, Int. J. Hydrogen Energy 45 (2020) 337–379, https://doi.org/10.1016/j.ijhydene.2019.07.070.
[37] Y. Xiao, T. Wang, G. Qiu, K. Zhang, C. Xue, B. Li, Synthesis of EDTA-bridged CdS/g-C3N4 heterostructure photocatalyst with enhanced performance for photoredox reactions, J. Colloid Interface Sci. 577 (2020) 459–470, https://doi.org/10.1016/j.jcis.2020.05.099.
[38] Y. Shang, T. Wang, Y. Xiao, Z. Dong, X. Li, B. Li, Constructing BiOBr/CoOx/g-C3N4 Z-scheme photocatalyst with CoOx as both redox mediator and cocatalyst for phenol degradation, J. Alloys Compd. 875 (2021), 159998, https://doi.org/10.1016/j.jallcom.2021.159998.
[39] Y. Xiao, X. Tao, G. Qiu, Z. Dai, P. Gao, B. Li, Optimal synthesis of a direct Z-scheme photocatalyst with ultrathin W 18 O 49 nanowires on g-C 3 N 4 nanosheets for solar-driven oxidation reactions, J. Colloid Interface Sci. 550 (2019) 99–109, https://doi.org/10.1016/j.jcis.2019.04.081.
[40] S. Noor, R.S. Haider, S. Noor, S. Sajjad, S.A. Khan Leghari, M. Mehboob, M. Long, Role of conductive channels via CQDs on NiO/g-C3N4 Z-scheme composite as a bi-functional photocatalyst, Int. J. Hydrogen Energy 47 (2022) 36517–36529, https://doi.org/10.1016/j.ijhydene.2022.08.207.
[41] Y. Jiao, Y. Li, J. Wang, Z. He, Z. Li, Exfoliation-induced exposure of active sites for g-C3N4/N-doped carbon dots heterojunction to improve hydrogen evolution activity, Mol. Catal. 497 (2020), 111223, https://doi.org/10.1016/j.mcat.2020.111223.
[42] X.C. Yang, Y.L. Yang, S.L. Zhang, Y.F. Liu, S.J. Fu, M. Zhu, J.F. Hu, Z.J. Zhang, J. T. Zhao, Facile synthesis of porous nitrogen doped carbon dots (NCDs)@g-C3N4 for highly efficient photocatalytic and anti-counterfeiting applications, Appl. Surf. Sci. 490 (2019) 592–597, https://doi.org/10.1016/j.apsusc.2019.05.367.
[43] Z. Zheng, F. Han, B. Xing, X. Han, B. Li, Synthesis of Fe3O4@CdS@CQDs ternary core–shell heterostructures as a magnetically recoverable photocatalyst for selective alcohol oxidation coupled with H2O2 production, J. Colloid Interface Sci. 624 (2022) 460–470, https://doi.org/10.1016/j.jcis.2022.05.161.
[44] R.X. Seng, L.L. Tan, W.P.C. Lee, W.J. Ong, S.P. Chai, Nitrogen-doped carbon quantum dots-decorated 2D graphitic carbon nitride as a promising photocatalyst for environmental remediation: a study on the importance of hybridization approach, J. Environ. Manage. 255 (2020), 109936, https://doi.org/10.1016/j.jenvman.2019.109936.
[45] Y. Wang, X. Liu, J. Liu, B. Han, X. Hu, F. Yang, Z. Xu, Y. Li, S. Jia, Z. Li, Y. Zhao, Carbon quantum dot implanted graphite carbon nitride nanotubes: excellent charge separation and enhanced photocatalytic hydrogen evolution, Angew. Chemie 130 (2018) 5867–5873, https://doi.org/10.1002/ange.201802014.
[46] T. Jin, C. Liu, F. Chen, J. Qian, Y. Qiu, X. Meng, Z. Chen, Synthesis of g-C3N4/CQDs composite and its photocatalytic degradation property for rhodamine B, Carbon Lett. 32 (2022) 1451–1462, https://doi.org/10.1007/s42823-022-00382-2.
[47] F.F. Hasan, N.A.W.M. Zahidi, V.S. Bahar, U.R.R.P. Remli, A.A. Aziz, Carbon quantum dots (CQDs) based composites photocatalyst for wastewater

purification, in: Mater. Sci. Forum. 1056 MSF, 2022, pp. 111–117, https://doi.org/10.4028/p-ftn9wh.
[48] S. Feng, T. Chen, Z. Liu, J. Shi, X. Yue, Y. Li, Z-scheme CdS/CQDs/g-C3N4 composites with visible-near-infrared light response for efficient photocatalytic organic pollutant degradation, Sci. Total Environ. 704 (2020), 135404, https://doi.org/10.1016/j.scitotenv.2019.135404.
[49] T. Zhao, Z. Xing, Z. Xiu, Z. Li, S. Yang, W. Zhou, Oxygen-doped MoS 2 Nanospheres/CdS quantum dots/g-C 3 N 4 nanosheets super-architectures for prolonged charge lifetime and enhanced visible-light-driven photocatalytic performance, ACS Appl. Mater. Interfaces 11 (2019) 7104–7111, https://doi.org/10.1021/acsami.8b21131.
[50] S. Wojtyła, K. Śpiewak, T. Baran, Synthesis, characterization and activity of doped graphitic carbon nitride materials towards photocatalytic oxidation of volatile organic pollutants emitted from 3D printer, J. Photochem. Photobiol. A Chem. 391 (2020), https://doi.org/10.1016/j.jphotochem.2020.112355.
[51] S. Sharma, V. Dutta, P. Raizada, A. Aslam, P. Khan, Environmental technology & innovation controllable functionalization of g-C 3 N 4 mediated all-solid-state (ASS) Z-scheme photocatalysts towards sustainable energy and environmental applications, Environ. Technol. Innov. 24 (2021), 101972, https://doi.org/10.1016/j.eti.2021.101972.
[52] V. Hasija, P. Raizada, A. Sudhaik, K. Sharma, A. Kumar, P. Singh, S. B. Jonnalagadda, V.K. Thakur, Recent advances in noble metal free doped graphitic carbon nitride based nanohybrids for photocatalysis of organic contaminants in water: a review, Appl. Mater. Today 15 (2019) 494–524, https://doi.org/10.1016/j.apmt.2019.04.003.
[53] H.B. Truong, S. Bae, J. Cho, J. Hur, Advances in application of g–C3N4–based materials for treatment of polluted water and wastewater via activation of oxidants and photoelectrocatalysis: a comprehensive review, Chemosphere 286 (2022), 131737, https://doi.org/10.1016/j.chemosphere.2021.131737.
[54] M. Zhang, Y. Yang, X. An, L. An Hou, A critical review of g-C3N4-based photocatalytic membrane for water purification, Chem. Eng. J. 412 (2021), 128663, https://doi.org/10.1016/j.cej.2021.128663.
[55] S. Nasir, M.Z. Hussein, Z. Zainal, N.A. Yusof, Carbon-based nanomaterials/allotropes: a glimpse of their synthesis, properties and some applications, Materials (Basel) 11 (2018) 1–24, https://doi.org/10.3390/ma11020295.
[56] D. Vaya, B. Kaushik, P.K. Surolia, Recent advances in graphitic carbon nitride semiconductor: structure, synthesis and applications, Mater. Sci. Semicond. Process. 137 (2022), 106181, https://doi.org/10.1016/j.mssp.2021.106181.
[57] P. Murugesan, J.A. Moses, C. Anandharamakrishnan, Photocatalytic disinfection efficiency of 2D structure graphitic carbon nitride-based nanocomposites: a review, J. Mater. Sci. 54 (2019) 12206–12235, https://doi.org/10.1007/s10853-019-03695-2.
[58] V. Devthade, D. Kulhari, S.S. Umare, Role of precursors on photocatalytic behavior of graphitic carbon nitride, Mater. Today Proc. 5 (2018) 9203–9210, https://doi.org/10.1016/j.matpr.2017.10.045.
[59] K. Li, M. Chen, L. Chen, S. Zhao, W. Xue, Z. Han, Y. Han, Synthesis of g-C3N4 derived from different precursors for photodegradation of sulfamethazine under visible light, Processes 11 (2023), https://doi.org/10.3390/pr11020528.
[60] G. Xin, Y. Meng, Pyrolysis synthesized g-C 3N 4 for photocatalytic degradation of methylene blue, J. Chem. 2013 (2013), https://doi.org/10.1155/2013/187912.
[61] C. Zhao, Z. Liao, W. Liu, F. Liu, J. Ye, J. Liang, Y. Li, Carbon quantum dots modified tubular g-C3N4 with enhanced photocatalytic activity for carbamazepine elimination: mechanisms, degradation pathway and DFT calculation, J. Hazard. Mater. 381 (2020), 120957, https://doi.org/10.1016/j.jhazmat.2019.120957.
[62] P. Thakur, P. Raizada, P. Singh, A. Kumar, A.A.P. Khan, A.M. Asiri, Exploring recent advances in silver halides and graphitic carbon nitride-based photocatalyst for energy and environmental applications, Arab. J. Chem. 13 (2020) 8271–8300, https://doi.org/10.1016/j.arabjc.2020.04.026.
[63] X. Wang, J. Cheng, H. Yu, J. Yu, A facile hydrothermal synthesis of carbon dots modified g-C3N4 for enhanced photocatalytic H2-evolution performance, Dalt. Trans. 46 (2017) 6417–6424, https://doi.org/10.1039/c7dt00773f.
[64] K.T. Wong, S.B. Jang, P. Saravanan, I.W. Nah, S. Park, J. Choi, C. Park, Y. Kim, Y. Yoon, M. Jang, Critical insight on the hydrothermal effects toward exfoliation of g-C 3 N 4 and simultaneous in-situ deposition of carbon quantum dots, Appl. Surf. Sci. 471 (2019) 703–713, https://doi.org/10.1016/j.apsusc.2018.12.064.
[65] C.H. Hak, K.H. Leong, Y.H. Chin, P. Saravanan, S.T. Tan, W.C. Chong, L.C. Sim, Water hyacinth derived carbon quantum dots and g-C3N4 composites for sunlight driven photodegradation of 2,4-dichlorophenol, SN Appl. Sci. 2 (2020) 1–14, https://doi.org/10.1007/s42452-020-2840-y.
[66] W. Liu, Y. Li, F. Liu, W. Jiang, D. Zhang, J. Liang, Visible-light-driven photocatalytic degradation of diclofenac by carbon quantum dots modified porous g-C3N4: mechanisms, degradation pathway and DFT calculation, Water Res. 151 (2019) 8–19, https://doi.org/10.1016/j.watres.2018.11.084.
[67] G. Yao, Y. Liu, J. Liu, Y. Xu, Facile synthesis of porous g-C3N4 with enhanced visible-light photoactivity, Molecules 27 (2022), https://doi.org/10.3390/molecules27061754.
[68] Q. Xu, D. Ma, S. Yang, Z. Tian, B. Cheng, J. Fan, Novel g-C3N4/g-C3N4 S-scheme isotype heterojunction for improved photocatalytic hydrogen generation, Appl. Surf. Sci. 495 (2019), 143555, https://doi.org/10.1016/j.apsusc.2019.143555.
[69] S. Panneri, P. Ganguly, M. Mohan, B.N. Nair, A.A.P. Mohamed, K.G. Warrier, U. S. Hareesh, Photoregenerable, bifunctional granules of carbon-doped g-C3N4 as adsorptive photocatalyst for the efficient removal of tetracycline antibiotic, ACS Sustain. Chem. Eng. 5 (2017) 1610–1618, https://doi.org/10.1021/acssuschemeng.6b02383.
[70] R. Tang Guo, J. Wang, Z. Xu Bi, X. Chen, X. Hu, W. Guo Pan, Recent advances and perspectives of g–C3N4–based materials for photocatalytic dyes degradation, Chemosphere 295 (2022), 133834, https://doi.org/10.1016/j.chemosphere.2022.133834.
[71] M. Lin, C. Wang, C. Liu, J. Fang, C. Chen, Graphitic-like carbon nitride nanosheets sensitized ZnO nanoparticles for enhanced catalytic activity under natural sunlight, Ferroelectrics 565 (2020) 99–107, https://doi.org/10.1080/00150193.2020.1761723.
[72] Y. Wang, Y. Li, J. Zhao, J. Wang, Z. Li, g-C 3 N 4 /B doped g-C 3 N 4 quantum dots heterojunction photocatalysts for hydrogen evolution under visible light, Int. J. Hydrogen Energy 44 (2019) 618–628, https://doi.org/10.1016/j.ijhydene.2018.11.067.
[73] Y. Chen, F. Su, H. Xie, R. Wang, C. Ding, J. Huang, Y. Xu, L. Ye, One-step construction of S-scheme heterojunctions of N-doped MoS2 and S-doped g-C3N4 for enhanced photocatalytic hydrogen evolution, Chem. Eng. J. 404 (2021), 126498, https://doi.org/10.1016/j.cej.2020.126498.
[74] H. Li, J. Zhao, Y. Geng, Z. Li, Y. Li, J. Wang, Construction of CoP/B doped g-C3N4 nanodots/g-C3N4 nanosheets ternary catalysts for enhanced photocatalytic hydrogen production performance, Appl. Surf. Sci. 496 (2019), 143738, https://doi.org/10.1016/j.apsusc.2019.143738.
[75] M.A. Mohamed, M.F.M. Zain, L.J. Minggu, M.B. Kassim, J. Jaafar, N.A. Saidina Amin, Z.A. Mohd Hir, M.S. Rosmi, Enhancement of visible light photocatalytic hydrogen evolution by bio-mimetic C-doped graphitic carbon nitride, Int. J. Hydrogen Energy 44 (2019) 13098–13105, https://doi.org/10.1016/j.ijhydene.2019.02.243.
[76] M.O. Fuentez-Torres, F. Ortiz-Chi, C.G. Espinosa-González, M. Aleman, A. Cervantes-Uribe, J.G. Torres-Torres, M.K. Kesarla, V. Collins-Martínez, S. Godavarthi, L. Martínez-Gómez, Facile synthesis of Zn doped g-C3N4 for enhanced visible light driven photocatalytic hydrogen production, Top. Catal. 64 (2021) 65–72, https://doi.org/10.1007/s11244-020-01298-9.
[77] X. Yang, X. Cao, B. Tang, B. Shan, M. Deng, Y. Liu, rGO/Fe-doped g-C 3 N 4 visible-light driven photocatalyst with improved NO removal performance, J. Photochem. Photobiol. A Chem. 375 (2019) 40–47, https://doi.org/10.1016/j.jphotochem.2019.02.011.
[78] X. Yang, Z. Tian, Y. Chen, H. Huang, J. Hu, B. Wen, In situ synthesis of 2D ultrathin cobalt doped g-C3N4 nanosheets enhances photocatalytic performance by accelerating charge transfer, J. Alloys Compd. 859 (2021), 157754, https://doi.org/10.1016/j.jallcom.2020.157754.
[79] S. Wojtyła, K. Śpiewak, T. Baran, Synthesis, characterization and activity of doped graphitic carbon nitride materials towards photocatalytic oxidation of volatile organic pollutants emitted from 3D printer, J. Photochem. Photobiol. A Chem. 391 (2020), 112355, https://doi.org/10.1016/J.JPHOTOCHEM.2020.112355.
[80] D. Gong, J. Guo, F. Wang, J. Zhang, S. Song, B. Feng, X. Zhang, W. Zhang, Green construction of metal- and additive-free citrus peel-derived carbon dot/g-C3N4 photocatalysts for the high-performance photocatalytic decomposition of sunset yellow, Food Chem. 425 (2023), 136470, https://doi.org/10.1016/j.foodchem.2023.136470.
[81] U.A. Rani, L.Y. Ng, C.Y. Ng, E. Mahmoudi, A review of carbon quantum dots and their applications in wastewater treatment, Adv. Colloid Interface Sci. 278 (2020), 102124, https://doi.org/10.1016/j.cis.2020.102124.
[82] M.J. Molaei, The optical properties and solar energy conversion applications of carbon quantum dots: a review, Sol. Energy 196 (2020) 549–566, https://doi.org/10.1016/j.solener.2019.12.036.
[83] M.J. Molaei, Carbon quantum dots and their biomedical and therapeutic applications: a review, RSC Adv. 9 (2019) 6460–6481, https://doi.org/10.1039/c8ra08088g.
[84] N.A. Mahat, S.A. Shamsudin, N. Jullok, A.H. Ma'Radzi, Carbon quantum dots embedded polysulfone membranes for antibacterial performance in the process of forward osmosis, Desalination 493 (2020), https://doi.org/10.1016/j.desal.2020.114618.
[85] G. Li, J. Huang, N. Wang, J. Huang, Y. Zheng, G. Zhan, Q. Li, Carbon quantum dots functionalized g-C3N4 nanosheets as enhanced visible-light photocatalysts for water splitting, Diamond Relat. Mater. 116 (2021), https://doi.org/10.1016/j.diamond.2021.108242.
[86] M. Shalahuddin Al Ja'farawy, A. Purwanto Kusumandari, H. Widiyandari, Carbon quantum dots supported zinc oxide (ZnO/CQDs) efficient photocatalyst for organic pollutant degradation – a systematic review, Environ. Nanotechnology, Monit. Manag. 18 (2022), 100681, https://doi.org/10.1016/j.enmm.2022.100681.
[87] M.E. Khan, A. Mohammad, T. Yoon, State-of-the-art developments in carbon quantum dots (CQDs): photo-catalysis, bio-imaging, and bio-sensing applications, Chemosphere 302 (2022), 134815, https://doi.org/10.1016/j.chemosphere.2022.134815.
[88] M. Saikia, T. Das, N. Dihingia, X. Fan, L.F.O. Silva, B.K. Saikia, Formation of carbon quantum dots and graphene nanosheets from different abundant carbonaceous materials, Diamond Relat. Mater. 106 (2020), 107813, https://doi.org/10.1016/j.diamond.2020.107813.
[89] M.H. Elsayed, J. Jayakumar, M. Abdellah, T.H. Mansoure, K. Zheng, A.M. Elewa, C.L. Chang, L.Y. Ting, W.C. Lin, H. Hua Yu, W.H. Wang, C.C. Chung, H.H. Chou, Visible-light-driven hydrogen evolution using nitrogen-doped carbon quantum dot-implanted polymer dots as metal-free photocatalysts, Appl. Catal. Environ. 283 (2021), 119659, https://doi.org/10.1016/j.apcatb.2020.119659.
[90] S.J. Phang, L.L. Tan, Recent advances in carbon quantum dot (CQD)-based two dimensional materials for photocatalytic applications, Catal. Sci. Technol. 9 (2019) 5882–5905, https://doi.org/10.1039/c9cy01452g.

[91] U.R.R.P. Remli, A.A. Aziz, Photocatalytic degradation of methyl orange using carbon quantum dots (CQDs) derived from watermelon rinds, IOP Conf. Ser. Mater. Sci. Eng. 736 (2020), https://doi.org/10.1088/1757-899X/736/4/042038.
[92] M.T. Genc, G. Yanalak, G. Arslan, I.H. Patir, Green preparation of carbon quantum dots using Gingko biloba to sensitize TiO2 for the photohydrogen production, Mater. Sci. Semicond. Process. 109 (2020), 104945, https://doi.org/10.1016/j.mssp.2020.104945.
[93] Y. Su, G. Liu, C. Zeng, Y. Lu, H. Luo, R. Zhang, Carbon quantum dots-decorated TiO2/g-C3N4 film electrode as a photoanode with improved photoelectrocatalytic performance for 1,4-dioxane degradation, Chemosphere 251 (2020), 126381, https://doi.org/10.1016/j.chemosphere.2020.126381.
[94] X. Miao, X. Yue, Z. Ji, X. Shen, H. Zhou, M. Liu, K. Xu, J. Zhu, G. Zhu, L. Kong, S. A. Shah, Nitrogen-doped carbon dots decorated on g-C3N4/Ag3PO4 photocatalyst with improved visible light photocatalytic activity and mechanism insight, Appl. Catal. Environ. 227 (2018) 459–469, https://doi.org/10.1016/j.apcatb.2018.01.057.
[95] A. Aghamali, M. Khosravi, H. Hamishehkar, N. Modirshahla, M.A. Behnajady, Synthesis and characterization of high efficient photoluminescent sunlight driven photocatalyst of N-carbon quantum dots, JOL 201 (2018) 265–274, https://doi.org/10.1016/j.jlumin.2018.04.061.
[96] Z. Peng, Y. Zhou, C. Ji, J. Pardo, K.J. Mintz, R.R. Pandey, C.C. Chusuei, R. M. Graham, G. Yan, R.M. Leblanc, Facile synthesis of "boron-doped" carbon dots and their application in visible-light-driven photocatalytic degradation of organic dyes, Nanomaterials 10 (2020) 1–17, https://doi.org/10.3390/nano10081560.
[97] P.M. Olmos-Moya, S. Velazquez-Martinez, C. Pineda-Arellano, J.R. Rangel-Mendez, L.F. Chazaro-Ruiz, High added value functionalized carbon quantum dots synthetized from orange peels by assisted microwave solvothermal method and their performance as photosensitizer of mesoporous TiO2 photoelectrodes, Carbon N. Y. 187 (2022) 216–229, https://doi.org/10.1016/j.carbon.2021.11.003.
[98] J.P. Malavika, C. Shobana, M. Ragupathi, P. Kumar, Y.S. Lee, M. Govarthanan, R. K. Selvan, A sustainable green synthesis of functionalized biocompatible carbon quantum dots from Aloe barbadensis miller and its multifunctional applications, Environ. Res. 200 (2021), 111414, https://doi.org/10.1016/j.envres.2021.111414.
[99] Q. Huang, X. Lin, J.J. Zhu, Q.X. Tong, Pd-au@carbon dots nanocomposite: facile synthesis and application as an ultrasensitive electrochemical biosensor for determination of colitoxin DNA in human serum, Biosens. Bioelectron. 94 (2017) 507–512, https://doi.org/10.1016/j.bios.2017.03.048.
[100] B. Li, Q. Fang, Y. Si, T. Huang, W.Q. Huang, W. Hu, A. Pan, X. Fan, G.F. Huang, Ultra-thin tubular graphitic carbon nitride-carbon dot lateral heterostructures: one-step synthesis and highly efficient catalytic hydrogen generation, Chem. Eng. J. 397 (2020), https://doi.org/10.1016/j.cej.2020.125470.
[101] Y. Zhang, W. De Zhang, Ternary catalysts based on amino-functionalized carbon quantum dots, graphitic carbon nitride nanosheets and cobalt complex for efficient H 2 evolution under visible light irradiation, Carbon N. Y. 145 (2019) 488–500, https://doi.org/10.1016/j.carbon.2019.01.052.
[102] H. He, L. Huang, Z. Zhong, S. Tan, Constructing three-dimensional porous graphene-carbon quantum dots/g-C 3 N 4 nanosheet aerogel metal-free photocatalyst with enhanced photocatalytic activity, Appl. Surf. Sci. 441 (2018) 285–294, https://doi.org/10.1016/j.apsusc.2018.01.298.
[103] C. Prasad, H. Tang, Q. Liu, I. Bahadur, S. Karlapudi, Y. Jiang, A latest overview on photocatalytic application of g-C3N4 based nanostructured materials for hydrogen production, Int. J. Hydrogen Energy 45 (2020) 337–379, https://doi.org/10.1016/j.ijhydene.2019.07.070.
[104] G. Zhang, Q. Ji, Z. Wu, G. Wang, H. Liu, J. Qu, J. Li, Facile "spot-heating" synthesis of carbon dots/carbon nitride for solar hydrogen evolution synchronously with contaminant decomposition, Adv. Funct. Mater. 28 (2018) 1–8, https://doi.org/10.1002/adfm.201706462.
[105] L.C. Sim, J.Y. Tai, K.H. Leong, P. Saravanan, S.T. Tan, W.C. Chong, A.A. Aziz, Metal free and sunlight driven g-C3N4 based photocatalyst using carbon quantum dots from Arabian dates: green strategy for photodegradation of 2,4-dichlorophenol and selective detection of Fe3+, Diamond Relat. Mater. 120 (2021), 108679 https://doi.org/10.1016/j.diamond.2021.108679.
[106] X. Miao, Z. Ji, J. Wu, X. Shen, J. Wang, L. Kong, M. Liu, C. Song, g-C3N4/AgBr nanocomposite decorated with carbon dots as a highly efficient visible-light-driven photocatalyst, J. Colloid Interface Sci. 502 (2017) 24–32, https://doi.org/10.1016/j.jcis.2017.04.087.
[107] B. Zhao, B. Wang, H. Lu, S. Dai, Z. Huang, Tuning the visible-light photocatalytic degradation activity of thin nanosheets constructed porous g-C3N4 microspheres by decorating ionic liquid modified carbon dots: roles of heterojunctions and surface charges, New J. Chem. 43 (2019) 10141–10150, https://doi.org/10.1039/c9nj00308h.
[108] X. Lin, C. Liu, J. Wang, S. Yang, J. Shi, Y. Hong, Graphitic carbon nitride quantum dots and nitrogen-doped carbon quantum dots co-decorated with BiVO4 microspheres: a ternary heterostructure photocatalyst for water purification, Sep. Purif. Technol. 226 (2019) 117–127, https://doi.org/10.1016/j.seppur.2019.05.093.
[109] J. Shi, S. Feng, T. Chen, Y. Li, Effect of porous modification on the synthesis and photocatalytic activity of graphitic carbon nitride/carbon quantum dot nanocomposite, J. Mater. Sci. Mater. Electron. 29 (2018) 17454–17462, https://doi.org/10.1007/s10854-018-9845-y.
[110] P. Matheswaran, P. Thangavelu, B. Palanivel, Carbon dot sensitized integrative g-C3N4/AgCl hybrids: an synergetic interaction for enhanced visible light driven photocatalytic process, Adv. Powder Technol. 30 (2019) 1715–1723, https://doi.org/10.1016/j.apt.2019.05.024.
[111] S. Asadzadeh-Khaneghah, A. Habibi-Yangjeh, M. Abedi, Decoration of carbon dots and AgCl over g-C3N4 nanosheets: novel photocatalysts with substantially improved activity under visible light, Sep. Purif. Technol. 199 (2018) 64–77, https://doi.org/10.1016/j.seppur.2018.01.023.
[112] J. Jia, X. Zhang, C. Jiang, W. Huang, Y. Wang, Visible-light-driven nitrogen-doped carbon quantum dots decorated g-C3N4/Bi2WO6 Z-scheme composite with enhanced photocatalytic activity and mechanism insight, J. Alloys Compd. 835 (2020), 155180, https://doi.org/10.1016/j.jallcom.2020.155180.
[113] S. Fang, Y. Xia, K. Lv, Q. Li, J. Sun, M. Li, Effect of carbon-dots modification on the structure and photocatalytic activity of g-C3N4, Appl. Catal. Environ. 185 (2016) 225–232, https://doi.org/10.1016/j.apcatb.2015.12.025.
[114] H. Li, G. Huang, H. Xu, Z. Yang, X. Xu, J. Li, A. Qu, Y. Chen, Enhancing photodegradation activity of g-C3N4 via decorating with S-doped carbon nitride quantum dots by in situ polymerization, J. Solid State Chem. 292 (2020), 121705, https://doi.org/10.1016/j.jssc.2020.121705.
[115] P. Wu, L. Feng, J. Liu, X. Zhang, S. Tian, H. Hu, C. Xu, G. Yin, Enhanced photocatalytic activity of Jamun-like Zn2V2O7/C-dots/g-C3N4 nanocomposites for rhodamine B degradation under the visible light radiation, J. Mater. Sci. Mater. Electron. 31 (2020) 1879–1890, https://doi.org/10.1007/s10854-019-02707-w.
[116] Q. Yang, S. Wei, L. Zhang, R. Yang, Ultrasound-assisted synthesis of BiVO4/C-dots/g-C3N4: Z-scheme heterojunction photocatalysts for degradation of minocycline hydrochloride and rhodamine B: optimization and mechanism investigation, New J. Chem. 44 (2020) 17641–17653, https://doi.org/10.1039/d0nj03375h.
[117] F.Y. Chen, L. Cheng, Y. Bin Tang, K.K. Shu, W.L. Shi, Construction of Z-scheme heterojunction g-C3N4/CQDs/InVO4 with broad-spectrum response for efficient rhodamine B degradation and H2 evolution under visible light, J. Chem. Technol. Biotechnol. 96 (2021) 3074–3083, https://doi.org/10.1002/jctb.6859.
[118] Z. Zhang, S. Lin, X. Li, H. Li, W. Cui, Metal free and efficient photoelectrocatalytic removal of organic contaminants over g-C3N4 nanosheet films decorated with carbon quantum dots, RSC Adv. 7 (2017) 56335–56343, https://doi.org/10.1039/c7ra11205j.
[119] Y. Zhou, A.E. ElMetwally, J. Chen, W. Shi, E.K. Cilingir, B. Walters, K.J. Mintz, C. Martin, B.C.L.B. Ferreira, W. Zhang, S.D. Hettiarachchi, L.F. Serafim, P. L. Blackwelder, A.H. Wikramanayake, Z. Peng, R.M. Leblanc, Gel-like carbon dots: a high-performance future photocatalyst, J. Colloid Interface Sci. 599 (2021) 519–532, https://doi.org/10.1016/j.jcis.2021.04.121.
[120] S. Asadzadeh-Khaneghah, A. Habibi-Yangjeh, K. Nakata, Decoration of carbon dots over hydrogen peroxide treated graphitic carbon nitride: exceptional photocatalytic performance in removal of different contaminants under visible light, J. Photochem. Photobiol. A Chem. 374 (2019) 161–172, https://doi.org/10.1016/j.jphotochem.2019.02.002.
[121] Y.Y. Li, Y. Si, B.X. Zhou, T. Huang, W.Q. Huang, W. Hu, A. Pan, X. Fan, G. F. Huang, Interfacial charge modulation: carbon quantum dot implanted carbon nitride double-deck nanoframes for robust visible-light photocatalytic tetracycline degradation, Nanoscale 12 (2020) 3135–3145, https://doi.org/10.1039/c9nr09945j.
[122] C. Wang, Y. Zhou, Y. Sun, G. Guo, Q. Fu, Z. Xiong, Y. Liu, Facile synthesis of nanoporpous graphitic carbon nitride photocatalyst coupled with N-doped graphene quantum dots for efficient photo-degradation dyes under nature solar light radiation, Diamond Relat. Mater. 89 (2018) 197–205, https://doi.org/10.1016/j.diamond.2018.09.012.
[123] X. Jian, X. Liu, H.M. Yang, J.G. Li, X.L. Song, H.Y. Dai, Z.H. Liang, Construction of carbon quantum dots/proton-functionalized graphitic carbon nitride nanocomposite via electrostatic self-assembly strategy and its application, Appl. Surf. Sci. 370 (2016) 514–521, https://doi.org/10.1016/j.apsusc.2016.02.119.
[124] J. Liu, H. Xu, Y. Xu, Y. Song, J. Lian, Y. Zhao, L. Wang, L. Huang, H. Ji, H. Li, Graphene quantum dots modified mesoporous graphite carbon nitride with significant enhancement of photocatalytic activity, Appl. Catal. Environ. 207 (2017) 429–437, https://doi.org/10.1016/j.apcatb.2017.01.071.
[125] J. Pan, M. You, C. Chi, Z. Dong, B. Wang, M. Zhu, W. Zhao, C. Song, Y. Zheng, C. Li, The two dimension carbon quantum dots modified porous g-C3N4/TiO2 nano-heterojunctions for visible light hydrogen production enhancement, Int. J. Hydrogen Energy 43 (2018) 6586–6593, https://doi.org/10.1016/j.ijhydene.2018.02.067.
[126] F. Wang, Y. Wang, Y. Feng, Y. Zeng, Z. Xie, Q. Zhang, Y. Su, P. Chen, Y. Liu, K. Yao, W. Lv, G. Liu, Novel ternary photocatalyst of single atom-dispersed silver and carbon quantum dots co-loaded with ultrathin g-C3N4 for broad spectrum photocatalytic degradation of naproxen, Appl. Catal. Environ. 221 (2018) 510–520, https://doi.org/10.1016/j.apcatb.2017.09.055.
[127] C. Vogt, J. Kranenborg, M. Monai, B.M. Weckhuysen, Structure sensitivity in steam and dry methane reforming over nickel: activity and carbon formation, ACS Catal. 10 (2020) 1428–1438, https://doi.org/10.1021/acscatal.9b04193.
[128] A. Nishimura, T. Takada, S. Ohata, M.L. Kolhe, Biogas dry reforming for hydrogen through membrane reactor utilizing negative pressure, Fuels 2 (2021) 194–209, https://doi.org/10.3390/fuels2020012.
[129] F.G.M. de Medeiros, F.W.B. Lopes, B. Rego de Vasconcelos, Prospects and technical challenges in hydrogen production through dry reforming of methane, Catalysts 12 (2022), https://doi.org/10.3390/catal12040363.
[130] K. Wang, X. Wang, H. Pan, Y. Liu, S. Xu, S. Cao, In situ fabrication of CDs/g-C3N4 hybrids with enhanced interface connection via calcination of the precursors for photocatalytic H2 evolution, Int. J. Hydrogen Energy 43 (2018) 91–99, https://doi.org/10.1016/j.ijhydene.2017.11.003.

[131] L. Li, X. Zhu, Enhanced photocatalytic hydrogen evolution of carbon quantum dot modified 1D protonated nanorods of graphitic carbon nitride, ACS Appl. Nano Mater. 1 (2018) 5337–5344, https://doi.org/10.1021/acsanm.8b01381.
[132] J. Qin, H. Zeng, Photocatalysts fabricated by depositing plasmonic ag nanoparticles on carbon quantum dots/graphitic carbon nitride for broad spectrum photocatalytic hydrogen generation, Appl. Catal. Environ. 209 (2017) 161–173, https://doi.org/10.1016/j.apcatb.2017.03.005.
[133] Q. Liu, T. Chen, Y. Guo, Z. Zhang, X. Fang, Ultrathin g-C3N4 nanosheets coupled with carbon nanodots as 2D/0D composites for efficient photocatalytic H2 evolution, Appl. Catal. Environ. 193 (2016) 248–258, https://doi.org/10.1016/j.apcatb.2016.04.034.
[134] D. Qu, J. Liu, X. Miao, M. Han, H. Zhang, Z. Cui, S. Sun, Z. Kang, H. Fan, Z. Sun, Peering into water splitting mechanism of g-C3N4-carbon dots metal-free photocatalyst, Appl. Catal. Environ. 227 (2018) 418–424, https://doi.org/10.1016/j.apcatb.2018.01.030.
[135] K. Li, F.Y. Su, W. De Zhang, Modification of g-C 3 N 4 nanosheets by carbon quantum dots for highly efficient photocatalytic generation of hydrogen, Appl. Surf. Sci. 375 (2016) 110–117, https://doi.org/10.1016/j.apsusc.2016.03.025.
[136] X.H. Jiang, L.C. Wang, F. Yu, Y.C. Nie, Q.J. Xing, X. Liu, Y. Pei, J.P. Zou, W.L. Dai, Photodegradation of organic pollutants coupled with simultaneous photocatalytic evolution of hydrogen using quantum-dot-modified g-C3N4 catalysts under visible-light irradiation, ACS Sustain. Chem. Eng. 6 (2018) 12695–12705, https://doi.org/10.1021/acssuschemeng.8b01695.
[137] Y. Li, X. Feng, Z. Lu, H. Yin, F. Liu, Q. Xiang, Enhanced photocatalytic H2-production activity of C-dots modified g-C3N4/TiO2 nanosheets composites, J. Colloid Interface Sci. 513 (2018) 866–876, https://doi.org/10.1016/j.jcis.2017.12.002.
[138] W. Liu, G. Liu, N. Shi, D. Liu, F. Wen, Carbon quantum dot-modified and chloride-doped ordered macroporous graphitic carbon nitride composites for hydrogen evolution, ACS Appl. Nano Mater. 3 (2020) 12188–12197, https://doi.org/10.1021/acsanm.0c02667.
[139] D. Zhang, W. Liu, P. Guo, Z. Wang, H. Xie, R. Wang, Z. Zhang, S. Qiu, Constructing MoS2-coupled carbon/g-C3N4 heterointerface to optimize charge delivery for enhanced photocatalytic capacity, J. Alloys Compd. 935 (2023), 168041, https://doi.org/10.1016/j.jallcom.2022.168041.
[140] F. Wang, P. Chen, Y. Feng, Z. Xie, Y. Liu, Y. Su, Q. Zhang, Y. Wang, K. Yao, W. Lv, G. Liu, Facile synthesis of N-doped carbon dots/g-C3N4 photocatalyst with enhanced visible-light photocatalytic activity for the degradation of indomethacin, Appl. Catal. Environ. 207 (2017) 103–113, https://doi.org/10.1016/j.apcatb.2017.02.024.
[141] L. Ai, R. Shi, J. Yang, K. Zhang, T. Zhang, S. Lu, Efficient combination of G-C3N4 and CDs for enhanced photocatalytic performance: a review of synthesis, strategies, and applications, Small 17 (2021) 1–31, https://doi.org/10.1002/smll.202007523.